AD-A187 180 VARIATION OF THE WIND STRESS RELATED TO FRONTAL PASSAGES DURING FASINEX ((U) NAVAL POSTGRADUATE SCHOOL MONTEREY CA J F MUNDY SEP 87 1/1

UNCLASSIFIED F/G 4/2 NL

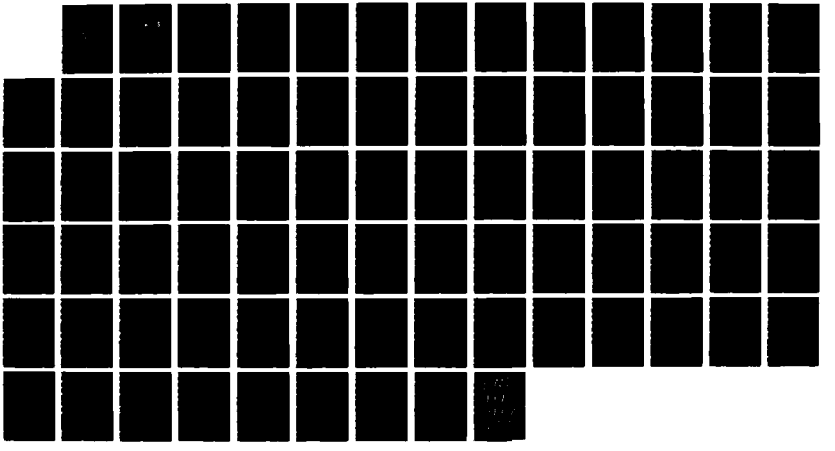

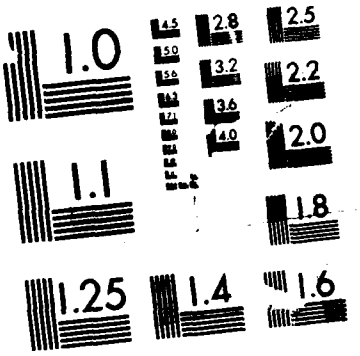

NAVAL POSTGRADUATE SCHOOL

Monterey, California

THESIS

VARIATION OF THE WIND STRESS RELATED TO FRONTAL PASSAGES DURING FASINEX 1986

by

James F. Mundy

September 1987

Thesis Advisor K. L. Davidson

UNCLASSIFIED
SECURITY CLASSIFICATION OF THIS PAGE

AD-A187180

REPORT DOCUMENTATION PAGE

1a REPORT SECURITY CLASSIFICATION: UNCLASSIFIED	1b RESTRICTIVE MARKINGS
2a SECURITY CLASSIFICATION AUTHORITY	3 DISTRIBUTION/AVAILABILITY OF REPORT: Approved for public release; distribution is unlimited
2b DECLASSIFICATION/DOWNGRADING SCHEDULE	
4 PERFORMING ORGANIZATION REPORT NUMBER(S)	5 MONITORING ORGANIZATION REPORT NUMBER(S)
6a NAME OF PERFORMING ORGANIZATION: Naval Postgraduate School; 6b OFFICE SYMBOL (If applicable): Code 63	7a NAME OF MONITORING ORGANIZATION: Naval Postgraduate School
6c ADDRESS (City, State, and ZIP Code): Monterey, CA 93943-5000	7b ADDRESS (City, State, and ZIP Code): Monterey, CA 93943-5000
8a NAME OF FUNDING/SPONSORING ORGANIZATION: Office of Naval Research; 8b OFFICE SYMBOL (If applicable)	9 PROCUREMENT INSTRUMENT IDENTIFICATION NUMBER
8c ADDRESS (City, State, and ZIP Code): 800 N. Quincy St. Arlington, VA 22217-5000	10 SOURCE OF FUNDING NUMBERS: PROGRAM ELEMENT NO; PROJECT NO; TASK NO; WORK UNIT ACCESSION NO

11 TITLE (Include Security Classification)

Variation of the Wind Stress Related to Frontal Passages During FASINEX 1986

12 PERSONAL AUTHOR(S)
Mundy, James F.

13a TYPE OF REPORT	13b TIME COVERED	14 DATE OF REPORT (Year, Month, Day)	15 PAGE COUNT
MASTER'S THESIS	FROM _____ TO _____	1987 September	76

16 SUPPLEMENTARY NOTATION

17 COSATI CODES			18 SUBJECT TERMS (Continue on reverse if necessary and identify by block number)
FIELD	GROUP	SUB-GROUP	Air-sea, wind stress, drag coefficient, wind-wave coupling, roughness length

19 ABSTRACT (Continue on reverse if necessary and identify by block number)

The variations of wind stress on the ocean surface during the passages of atmospheric cold fronts are investigated using data collected during the 1986 Frontal Air-Sea Interaction Experiment (FASINEX). Six frontal passages were observed from two ships (R/V's Oceanus and Endeavor) in the western North Atlantic during the period 14 February-6 March 1986. Wind stresses are calculated by both the dissipation method, using velocity variances measured with hot-film anemometers, and the bulk method, using mean wind, temperature, and humidity and a drag coefficient. The ratio of dissipation to bulk stress is found to be enhanced by a factor of up to 1.4 within approximately 200 km of a frontal zone when averaged over six frontal passages. The enhancement during individual frontal passages was as high as 3.6, with the major peaks occurring from 300 km ahead of the front to 400 km behind the front. Investigation of the differences in direction between surface wind and sea swell suggests that the enhancement is produced in large part through a combination of two factors: modulation of high-frequency wind waves by underlying swell and chaotic seas resulting from radiation of swell waves generated in the cold sector through the front.

20 DISTRIBUTION/AVAILABILITY OF ABSTRACT	21 ABSTRACT SECURITY CLASSIFICATION	
☒ UNCLASSIFIED/UNLIMITED ☐ SAME AS RPT ☐ DTIC USERS	UNCLASSIFIED	
22a NAME OF RESPONSIBLE INDIVIDUAL: Prof. K.L. Davidson, Dept. of Meteorology	22b TELEPHONE (Include Area Code): (408)-646-2309	22c OFFICE SYMBOL: Code 63Ds

DD FORM 1473, 84 MAR — 83 APR edition may be used until exhausted; All other editions are obsolete — SECURITY CLASSIFICATION OF THIS PAGE

Approved for public release; distribution is unlimited.

Variation of the Wind Stress Related to Frontal Passages During FASINEX 1986

by

James F. Mundy
Lieutenant Commander, United States Navy
B.S., University of Utah, 1975

Submitted in partial fulfillment of the
requirements for the degree of

MASTER OF SCIENCE IN METEOROLOGY AND OCEANOGRAPHY

from the

NAVAL POSTGRADUATE SCHOOL
September 1987

Author: _____
James F. Mundy

Approved by: _____
K.L. Davidson, Thesis Advisor

_____
W.J. Shaw, Second Reader

_____
R. J. Renard, Chairman,
Department of Meteorology

_____
G.E. Schacher,
Dean of Science and Engineering

ABSTRACT

The variations of wind stress on the ocean surface during the passages of atmospheric cold fronts are investigated using data collected during the 1986 Frontal Air-Sea Interaction Experiment (FASINEX). Six frontal passages were observed from two ships (R/V's Oceanus and Endeavor) in the western North Atlantic during the period 14 February-6 March 1986. Wind stresses are calculated by both the dissipation method, using velocity variances measured with hot-film anemometers, and the bulk method, using mean wind, temperature, and humidity and a drag coefficient. The ratio of dissipation to bulk stress is found to be enhanced by a factor of up to 1.4 within approximately 200 km of a frontal zone when averaged over six frontal passages. The enhancement during individual frontal passages was as high as 3.6, with the major peaks occurring from 300 km ahead of the front to 400 km behind the front. Investigation of the differences in direction between surface wind and sea swell suggests that the enhancement is produced in large part through a combination of two factors: modulation of high-frequency wind waves by underlying swell and chaotic seas resulting from radiation of swell waves generated in the cold sector through the front.

TABLE OF CONTENTS

LIST OF TABLES

LIST OF FIGURES

I. INTRODUCTION

Understanding and quantifying the momentum transfer occurring at the turbulent air-sea interface is important for the modeling and prediction of phenomena such as wave field development, whitecapping, and ocean mixed-layer depths. These phenomena also affect other practical applications, such as satellite remote sensing of winds and ocean acoustic forecasting. For example, Geernaert (1987) varied the drag coefficient (a measure of the efficiency of momentum transfer from the atmosphere to the ocean) by 30% in a coupled atmosphere-ocean boundary layer model, surface wave models, and a satellite scatterometer algorithm. He found that this resulted in 15% variations in both marine atmospheric boundary layer (MABL) height and oceanic boundary layer (OBL) depth, 15% to 30% variations in predicted wave heights, and 15% variations in both predicted whitecap coverage and scatterometer-derived winds. The 30% variation Geernaert used for the drag coefficient is conservative; as will be shown below, larger errors in the drag coefficient are possible if all parameters are not included when specifying its value. This may be particularly true when the vector wind and vector wave fields are complex.

The wind stress, τ, represents the vertical momentum flux from atmosphere to ocean, and is defined by

$$\tau = -\rho\overline{u'w'}, \tag{1.1}$$

where u' and w' are the longitudinal and vertical components, respectively, of the wind velocity fluctuations and ρ is the air density. A bulk formulation for τ as a function of an easily measured variable, the 10-meter wind speed u_{10}, is

$$\tau = \rho C_d u_{10}^2 \tag{1.2}$$

where C_d is the drag coefficient. Businger, *et al.* (1971) showed a relation between C_d and atmospheric stability. Other researchers have shown that C_d over the ocean also depends on wind speed (Large and Pond, 1981) and wave state (Kitaigorodskii, 1973; Byrne, 1982; Donelan, 1982; Hsu, 1974).

Recent investigations, using wind stresses derived from turbulent kinetic energy dissipation rates rather than bulk formulations, have shown stress variations which are not adequately explained using the bulk formulae with current formulations of C_d which take into account stability and wind speed dependencies. Boyle, *et al.* (1987) found that the bulk stress values based on an existing formulation were two to three times too low in pre-frontal, pre-trough and pre-ridge regions of transiting synoptic systems in the Gulf of Alaska during the Storm Transfer and Response Experiment (STREX). They suggested wind-wave interaction as the cause but did not have sufficient wave data to quantify this observed effect. Geernaert, *et al.* (1986b) found drag coefficients higher than the bulk values by a factor of 1.2, 1 h prior to a frontal passage during the Marine Remote Sensing (MARSEN) experiment. They speculate on two possible mechanisms for the stress enhancement: spatial modulation of high-frequency ocean wave energy by low-frequency swell and the effects of chaotic seas occurring due to wave convergence ahead of the front.

This thesis concerns results derived from an extensive data set collected during the Frontal Air-Sea Interaction Experiment (FASINEX) from 14 February through 6 March 1986. Fig. 1.1 shows the FASINEX study area. During this period six frontal passages occurred, and continuous records of air and sea temperatures, surface pressure, humidity, wind, and other meteorological parameters were collected on two ships, the R/V Oceanus and the R/V Endeavor. The Endeavor also provided an hourly record of swell height and direction obtained from bridge observations. The purpose of the analysis presented here is to identify the stress variations occurring during each frontal passage, and to seek indications of the mechanisms causing these variations.

Chapter II is a presentation of background on the bulk and dissipation methods of stress calculations, including recent attempts to model C_d to include wind-wave coupling. Chapter III covers the data collection, editing, and processing methods employed for this study. Chapter IV describes the individual frontal passages, presenting a synoptic summary and spatial cross-sections of the ratio of dissipation to bulk stress, swell height, and wind-swell direction difference for each front. The stress ratio variations seen in the cross-sections are related to synoptic events. Chapter V presents cumulative results for all six frontal passages. Chapter VI presents conclusions and suggests avenues for future research.

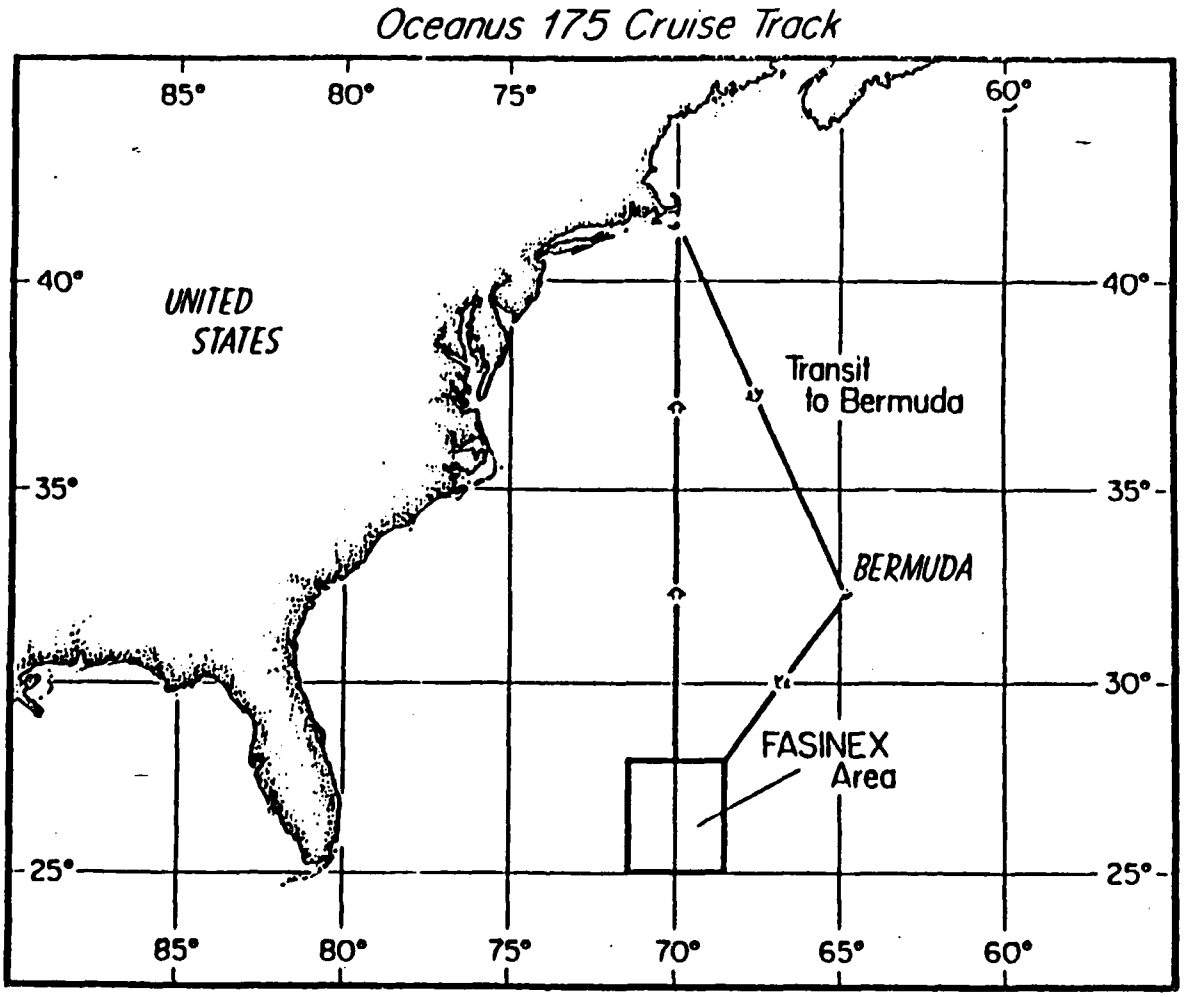

Fig. 1.1 FASINEX Study Area (Pennington and Weller, 1986).

II. BACKGROUND

A. BULK WIND STRESS FORMULATIONS

Identification of the wind stress enhancement due to variations other than those of wind speed and atmospheric stability requires that non-bulk derived stress values be normalized properly. This normalization is performed by using the bulk method based on a stability and wind speed dependent drag coefficient, C_d, as shown in (1.2). Variations in wind stress not related to u_{10}^2 must be accounted for in this formulation by varying the drag coefficient C_d as conditions change. Variations of C_d with atmospheric stability and wind speed are fairly well established. More recently, various investigators have focused on the dependence of C_d on sea state. Each of these dependencies will be discussed briefly below.

1. Atmospheric Stability Dependence of C_d

Businger, *et al.* (1971) found that in the surface layer, defined as the region in which the variations in stress are small compared to the surface value, the wind speed gradient could be defined as

$$\partial u/\partial z = (u_*/kz)\, \varphi_m(z/L), \tag{2.1}$$

where k is the von Karman constant (0.4), z is the height above the surface, L is the Monin-Obukhov length, and u_* is the friction velocity, defined by

$$u_* = (\overline{-u'w'})^{1/2}. \tag{2.2}$$

The parameter z/L is a measure of the atmospheric stability, and the stability function $\varphi_m(z/L)$ was formulated by Businger, *et al.* (1971) to be

$$\varphi_m(z/L) = (1 - 16\, z/L)^{-1/4},\ z/L < 0 \text{ (unstable), and} \tag{2.3}$$
$$\varphi_m(z/L) = 1 + 5\, z/L,\ z/L > 0 \text{ (stable).}$$

Integrating the wind speed gradient profile between a lower limiting height z_0, called the roughness length, and z gives a wind speed profile:

$$u(z) = u_* / k \, [\ln(z/z_0) - \psi(z/L)]. \qquad (2.4)$$

Here ψ is a stratification function, the graph of which is shown in Fig. 2.1. The drag coefficient for a given height, z, is then given by

$$C_d^{1/2} = k \, [\ln(z/z_0) - \psi(z/L)]^{-1}. \qquad (2.5)$$

It can be seen from this formula and Fig. 2.1 that C_d increases slowly as conditions change from unstable to neutral, and more rapidly under stable conditions as stability increases.

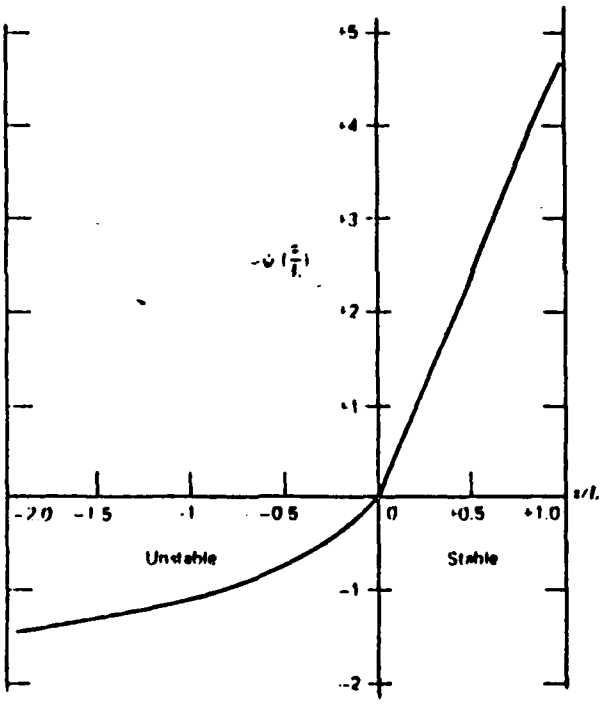

Fig. 2.1 Stratification function $\psi(z/L)$
(Haltiner and Williams, 1980).

2. Wind Speed and Sea State Dependence of C_d

A wind speed dependence of C_d was sought by previous investigators because of the fact that surface roughness of scales important in air-sea momentum transfer is associated with capillary waves, which change with wind speed.

Waves on the sea surface are assumed to act as roughness elements for the momentum transfer from atmosphere to ocean. The roughness length, z_0, and thus the drag coefficient (2.5) should therefore depend upon the state of the wave field. The problem of modeling the wind stress magnitude then hinges on selecting the length and height scales which are most important in the momentum transfer process (Geernaert, *et al.*, 1986b). Charnock (1955) developed, by dimensional analysis, a relation between the roughness length and the friction velocity:

$$z_0 = a\, u_*/g. \tag{2.7}$$

However, the supposedly constant coefficient a was found to vary depending on the characteristics of the water surface, leading Hsu (1974) to define a new Charnock coefficient according to the length and height scales of the dominant wind wave. Others (Byrne, 1982; Kitaigorodskii, 1973) have proposed roughness length parameterizations based on the integrated wave slope spectrum. Donelan (1982) set forth a drag coefficient formulation with separate contributions from both the low- and high-frequency portions of the wave spectrum. (Geernaert, *et al.*, 1986b)

Large and Pond (1981) found that the drag coefficient under neutrally stable conditions could be characterized as a function of the 10-meter wind speed u_{10}. Their estimates are:

$$\begin{aligned} 10^3\, C_{dn10} &= 1.2, \quad 4\ ms^{-1} < u_{10} < 11\ ms^{-1}, \text{ and} \\ 10^3\, C_{dn10} &= 0.49 + .065\, u_{10}, \quad 11\ ms^{-1} < u_{10} < 25\ ms^{-1}. \end{aligned} \tag{2.6}$$

Bulk neutral drag coefficients for this study were obtained using this formulation. These were corrected for stability according to (2.3), and then used to calculate the bulk wind stress from (1.2).

Because of the lack of wave spectrum data, more detailed sea state-dependent formulations were not used in the calculation of bulk wind stresses for this study. It is possible that, had this been done, a closer correspondence between bulk and dissipation stress values would have been found.

B. FACTORS CAUSING ENHANCED WIND STRESS NEAR AN ATMOSPHERIC FRONT

Processes which enhance observed wind stress near a front, through mechanisms other than wind speed increases, are poorly understood. Wind stresses near a front have been observed (Boyle, *et al.*, 1987) to be higher by a factor of 3 to 4 than those predicted by the bulk method with appropriate stability and wind speed factors applied. Although Byrne (1982) reports that his model predicted cold sector drag coefficients well for two storms sampled during STREX, limited information is available concerning the performance of sea state-dependent drag coefficient models under frontal zone conditions.

Geernaert, *et al.* (1986b) suggest two mechanisms for the enhancement of wind stress near a front. The first of these is spatial modulation of the high-frequency wind waves by underlying low-frequency swell. Phillips and Banner (1974) found through wind-tunnel experiments that the presence of wind drift and swell propagating in the same direction as the high-frequency wind waves reduces the amplitude the short waves can attain before breaking. The breaking rate of the high-frequency waves then increases near the crests of the long waves, resulting in increased momentum entrainment into the sea surface. Geernaert, *et al.* (1986a) also point out that the short-wave roughness elements generally assumed to be responsible for most of the momentum transfer will be elevated considerably on the long-wave crests and thus the wind shear above the wave will depend on the long-wave height.

When swell propagates nearly opposite the wind direction, the breaking rate of short waves is reduced, which could lead to a decrease in momentum transfer and wind stress. However, Geernaert, *et al.* (1986b) point out that in this case nonlinear energy transfer should act to steepen the waves, resulting in greater surface roughness and tending to offset the first effect.

The effects of dynamic modulation of short waves by swell would be expected to vary with the difference between the wind direction and the swell direction. The greatest effects should occur when wind and swell are in the same or opposite directions, with little effect when they are perpendicular. Based on the wave breaking phenomenon, the stress enhancement should be greatest with wind and swell in the same direction, and least when the directions are opposite. The signatures of this mechanism in the cross-sections investigated in this paper are a change in stress ratio associated with a change in swell height but not in swell direction, or a change associated with swell propagating with or against the wind.

The second mechanism proposed by Geernaert, *et al.* (1986b) for the enhancement of stress near a front is the effect of chaotic seas resulting from wave convergence ahead of the front. They argue that swell generated behind the front will travel through the front, while waves generated ahead of the front will not, as winds there are nearly parallel to the frontal zone. The interaction of the swell radiating from the cold sector with the existing warm sector wave field results in a more energetic sea ahead of the front, with larger wave amplitudes, steeper gravity waves, and more wave breaking. This would result in increased momentum transfer into the ocean ahead of the front. This effect should be most evident in the data when the dominant swell direction is nearly perpendicular to the wind direction, indicating the presence of independently-generated wave trains from behind and ahead of the front. The signature of this mechanism in the frontal cross-sections is a change in stress associated with a change toward perpendicularity in the wind-swell direction difference.

The two mechanisms discussed above are not mutually exclusive. They can both occur at the same time, particularly when the swell has significant components both parallel and perpendicular to the wind direction. In the discussion of the frontal cross-sections, an attempt will be made to determine which mechanism is most important for each major variation of the stress ratio. However, since purely parallel or perpendicular cases are rare, it is expected that some summation of the two effects is responsible for the majority of the stress variations.

III. DATA ACQUISITION, EDITING, AND PROCESSING

A. THE FRONTAL AIR-SEA INTERACTION EXPERIMENT

FASINEX was an international project conducted during the period 13 February-10 March 1986 in the Atlantic subtropical convergence zone near Bermuda (62° W to 72° W and 26 ° N to 30° N). The FASINEX area is shown in Fig. 1.1. The objectives of the experiment were to study the response of the upper ocean to atmospheric forcing in the vicinity of an oceanic front, the response of the lower atmosphere in that vicinity to the oceanic front, and the associated two-way interaction between atmosphere and ocean (Pennington and Weller, 1986). Meteorological and oceanic measurements were made during the experiment by satellite remote sensing, a moored buoy array, surface ships, and aircraft. The data examined in this study were acquired from two ships, the R/V Oceanus and the R/V Endeavor, during the period 14 February-6 March 1986 for analysis by the Environmental Physics Group (EPG) at the Naval Postgraduate School (NPS) in Monterey, California. One objective of the EPG analysis was to obtain wind stress measurements as a function of surface layer stability, vector wind and wave differences, and sea state.

B. DATA ACQUISITION

Table 1 lists the measurements made and instruments used on each ship. The instrument array on the Endeavor was located 14 m above sea level. On the Oceanus, temperature and humidity were measured at 6 m, and wind data were measured at 11.5 m above sea level.

All input signals from the instrument array were continuously sampled by an HP series 200 computer and stored on floppy disks. A model 400 Mini-Ubiquitous spectrum analyzer was used to produce real-time power spectral densities from the turbulent sensors (hot film and miniature cups).

The measurements of importance for this study are sea-surface temperature, mean surface layer wind, temperature, and humidity, and turbulent kinetic energy dissipation as measured by the hot film anemometer. Sea-surface temperature was measured continuously on the Endeavor using a thermistor suspended from a boom and lowered to a position just below the sea surface at steaming speed, and on the Oceanus a bucket thermometer was read at 15-min intervals. Mean surface layer wind

TABLE 1

FASINEX METEOROLOGICAL MEASUREMENTS

Measurements made on both ships indicated by *; others on Endeavor only.

Measurements	*Sensor/System*	*Frequency*
Radiation (down)	Long/short wave radiometers	Continuous
Sea Surface Temperature	Floating thermistor	Continuous
Mean Surface Layer:		
* Wind (speed, direction)	Cup anemometer, bivane	Continuous
Temperature	Resistance thermometer	Continuous
Humidity	Cool mirror	Continuous
Aerosols	Optical counters	Continuous
* Turbulent kinetic energy dissipation rate	Hot film, miniature cups	Continuous
Humidity variance dissipation rate	Lyman-α	Continuous
* Inversion height	SODAR	Continuous
* Temperature, humidity, and wind profiles	Radiosonde	2-6/day

speed measurements used in this study were obtained from cup anemometers of the optical chopper type, and wind directions from a standard vane with a 360° potentiometer. Air temperature was measured with a platinum resistance thermometer. Dew point was measured using a cooling mirror. The mirror normally closes an optical circuit. When it is cooled to the dew point temperature, dew forms on it and opens the circuit. A servo loop is used to maintain the mirror temperature at the dew point. All of these instruments were shielded from radiation and aspirated. The hot film anemometer measures wind speed by sensing the current needed to maintain the film at a constant temperature and balance the energy lost due to convective cooling by the wind. Ship speed and direction were also required so as to adjust the observed vector relative winds to their true wind equivalents. (Skupniewicz, *et al.*, 1986)

C. DATA EDITING

The variance spectra for the hot film measured velocities were affected by flow distortion during periods where the relative wind direction was not within ±90° of the bow of the ship. During periods of low relative wind speed, heat from the hot film itself produces convective turbulence and erroneous velocity variance spectra. Radio

interference, fog, sea spray, and rain also produce anomalous hot film signals. All data affected by such factors were eliminated from the data set. The remaining power spectra showed little evidence of contamination over the range of frequencies from 5 Hz to 20 Hz.

On both ships the turbulence statistics were based on 10-min averages. The stress calculations from the Endeavor data were made using 20-min averages. On the Oceanus, however, the air temperature, humidity, and relative wind direction measurements were made at 15- or 30-min intervals. The dissipation of turbulent kinetic energy was therefore calculated using 10-min averaged data, then averaged and merged with the meteorological data to produce 30-min averaged stress values for the Oceanus.

D. CALCULATION OF THE TURBULENT KINETIC ENERGY DISSIPATION RATE

The variance of fluctuations of horizontal wind velocity in the inertial subrange of isotropic turbulence can be characterized using the Kolmogoroff spectrum:

$$S_u(k) = \alpha \varepsilon^{2/3} k^{-5/3}, \tag{3.1}$$

where k is the eddy turbulent wave number, α is a constant evaluated by Champagne, *et al.* (1977) as 0.51, and $S_u(k)$ is the wave number-dependent variance spectral density function. Using Taylor's hypothesis for frozen turbulence, wave number and frequency are related by

$$k = 2\pi f / u_{rel}, \tag{3.2}$$

where f is the frequency and u_{rel} is the relative wind speed. Then the frequency-dependent spectral density is given by

$$S_u(f) = \alpha \varepsilon^{2/3} (2\pi/u_{rel})^{-2/3} f^{-5/3}, \tag{3.3}$$

since

$$k\, S(k) = f\, S(f). \tag{3.4}$$

A typical hot film spectrum is shown in Fig. 3.1.

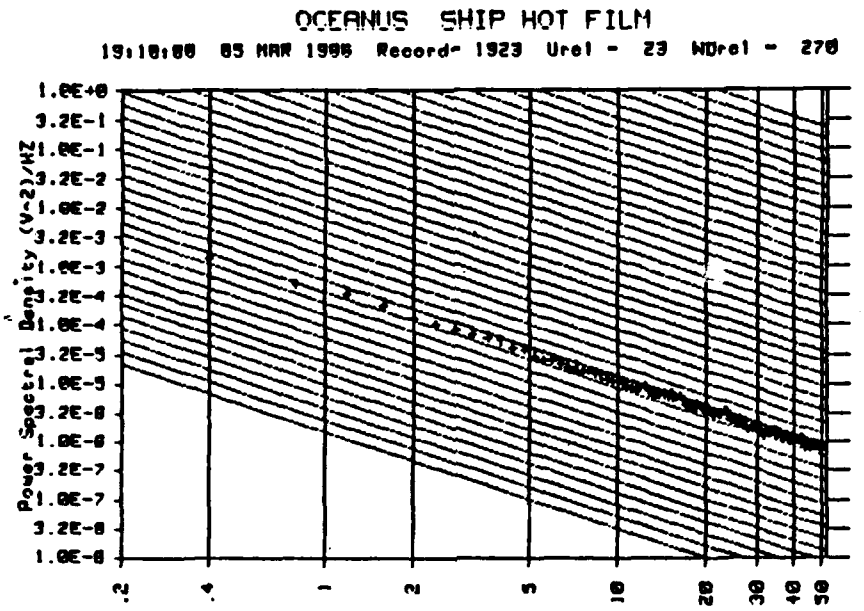

Fig. 3.1 Typical hot film variance spectrum.

A hot film equation relating the mean and fluctuating wind velocities to the mean and fluctuating voltages is

$$u'^2 = (4v_{bar}u_{rel}{}^{1/2}v'^2/B \times Gain)^2, \tag{3.5}$$

where u'^2 represents the velocity fluctuations, v_{bar} the mean hot film voltage, v'^2 the voltage fluctuation, B a hot film calibration, and Gain an instrument constant. B is calculated for each ten-min period and is the slope of the regression line between u_{rel} and v_{bar}.

Combining (3.4) and (3.5) yields

$$S_u(f) = 8u_{rel}{}^2v_{bar}{}^2P_{sd}/(\pi B^2 Gain^2), \tag{3.6}$$

where P_{sd} is $S_v(f)$, the measured hot film power spectrum density.

Combining (3.3) and (3.6) and solving for ε yields

$$\varepsilon = 1104\, u_{rel}{}^{1/2}v_{bar}{}^{3}B^{-3}f^{5/2}P_{sd}{}^{3/2}Gain^{-3}. \tag{3.7}$$

E. WIND STRESS FROM TURBULENT KINETIC ENERGY DISSIPATION

The friction velocity, u_*, can be estimated from the turbulent kinetic energy dissipation rate using an assumed turbulent kinetic energy balance relation and surface similarity for a flux-profile relation. Based on the assumption that in the surface layer, mechanical and buoyant production of turbulent kinetic energy balances dissipation, the steady state turbulent kinetic energy equation becomes

$$u_*^2 \partial u/\partial z + g\,(\overline{w' T_v'}/T_0) - \varepsilon = 0, \tag{3.8}$$

where u is mean wind speed, z is the measurement height, T_v' is the fluctuating virtual temperature, and T_0 is the surface temperature. With these assumptions, surface layer similarity yields the following general relation (Wyngaard and Cote, 1971):

$$u_* = [\varepsilon k z / \varphi_\varepsilon(z/L)]^{1/3}, \tag{3.9}$$

where k is the von Karman constant, L the Monin-Obukhov length, and φ_ε a dimensionless stability function. Values of φ_ε used for these calculations are from Wyngaard and Cote (1971) for the stable case and McBean and Elliot (1975) for the unstable case.

Since u_* is a function of z/L, which also depends on u_*, an iterative process was used to estimate u_* through the following equations:

$$Q_* = k(Q-Q_0)/[\ln(z_Q/z_{0Q}) - \psi_Q(z/L)], \tag{3.10}$$

$$T_* = k(T-T_0)/[\ln(z_T/Z_{0T}) - \psi_h(z/L)],$$

$$T_{*_V} = T_* + 0.00061(Q_* T),$$

$$z/L = kzgT_{*_V}/u_* T,$$

where z_T and z_Q are the temperature and humidity measurement heights. The corresponding roughness lengths z_{0T} and z_{0Q} were assumed equal and set to 2×10^{-5} m. The integral diabatic terms for humidity (ψ_Q) and temperature (ψ_h) were assumed equal and based on the formulation of Large and Pond (1981).

The dissipation stress was then calculated using the equation

$$\tau = \rho u_*^2. \tag{3.11}$$

Guest and Davidson (1987) compared wind stress values estimated by the dissipation method with those estimated by eddy correlation using sonic anemometer wind measurements and by the profile method using wind speed and temperature measurements made on a tower. They found excellent agreement between the results from the three methods, as shown in Fig. 3.2, which indicates that the dissipation method provides accurate estimates of the actual wind stress.

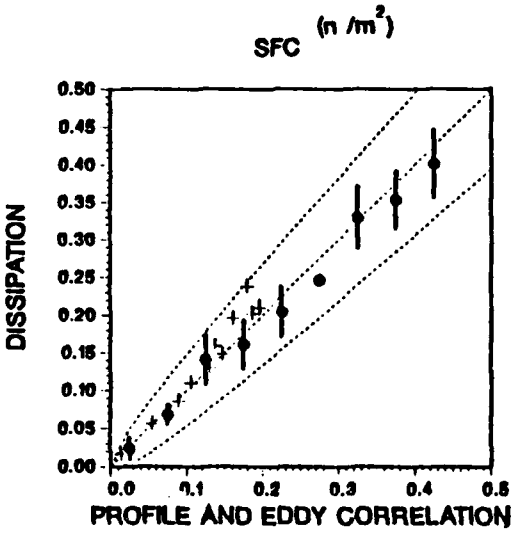

Fig. 3.2 Comparison of dissipation, profile, and eddy correlation derived wind stress (Guest and Davidson, 1987).

F. BULK STRESS CALCULATION

The bulk stress was calculated using equation 1.2. The neutral drag coefficient used was the stability-corrected wind speed-dependent formulation of Large and Pond (1981). The stability correction was based on the formulation by Businger, *et al.* (1971), as given by (2.3).

G. FRONTAL CROSS-SECTION DETERMINATION

To facilitate intercomparison of the data obtained by the two ships with respect to the frontal position, it was necessary to develop a presentation which compensated for the differences in frontal passage times and speeds of frontal movements relative to the two ships. Except for the ship positions, the data were obtained as time series. The procedure was to construct spatial cross sections of stress ratio, wind-swell direction difference, and swell height versus distance from the front for each frontal passage on each ship. The frontal cross-sections were determined using an assumed constant speed of movement of each front relative to each ship. The relative speeds were determined by measuring the distance between the front and each ship on the weather charts at two times bracketing the frontal passage, and calculating the average relative motion during this period (usually 12 or 24 h). This speed was then used to determine the distances from the front for the entire cross-section. Since the speeds of frontal movement were large compared to the ship speeds, this approximation appears to have produced consistent results even when the ships followed widely different tracks. The correspondence of events in the cross-sections from the two ships is excellent in every case.

IV. SYNOPTIC SUMMARIES AND FRONTAL CROSS-SECTIONS

A. GENERAL DISCUSSION

During the period from 14 February though 6 March 1986, six cold fronts passed though the FASINEX area. With two instrumented ships (R/V Oceanus and R/V Endeavor) as platforms, an unusual opportunity existed to examine the changes in wind stress associated with frontal passages.

This chapter describes the variations observed during frontal passages. The descriptions are of the synoptic conditions which occurred during the period, the ship positions and movements of the ships with respect to the fronts, and the cross-sections relative to each front of wind-swell direction difference, swell height, and ratio of dissipation to bulk stress acquired during each frontal passage. In the frontal cross-sections, the pre- and post-frontal distances are based on an assumed constant speed of movement of each front relative to each ship. Frontal speed variations and ship movements cause these distances to be estimates. However, there were no differences in the cross-sections from the two ships which could be attributed to the differences in the ship tracks. In all cases, features observed in the cross-section from one ship are also seen in that from the other ship at nearly the same distance. The air temperature, sea-level pressure, and wind data discussed are from Endeavor unless otherwise noted. All swell heights and wind-swell direction differences are also based on Endeavor data, since the record from Endeavor was much more complete than that from Oceanus.

Each frontal passage will be discussed in a separate section. The discussion will include the day of the frontal passage and the preceding and following days.

B. THE FRONTAL PASSAGE OF 15 FEBRUARY 1986

This was the fastest-moving front observed during the FASINEX period, with translation speeds of over 70 km/h relative to the two ships. It was a moderately strong front in terms of thermal contrast, with a drop of over 2° C in air temperature accompanying the frontal passage.

The sea-level pressure maps for the period 14 February-16 February are shown in Fig. 4.1. The synoptic scale patterns and ship movements for each day of the period will be discussed separately below.

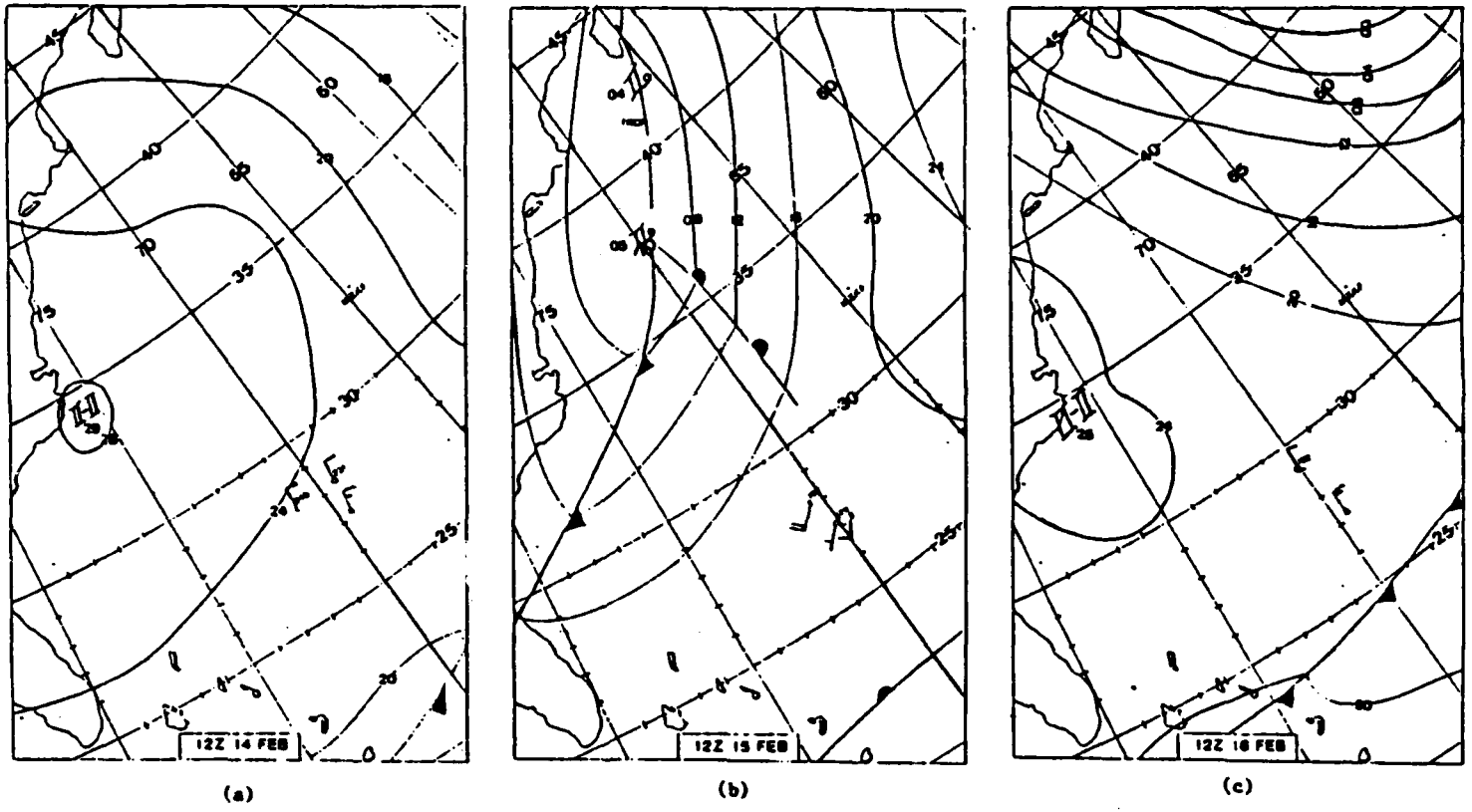

(a) (b) (c)

Fig. 4.1 Sea-level Pressure Maps for 14 Feb (a), 15 Feb (b), 16 Feb (c) 1986.

1. **Synoptic Discussion, 14-16 February**

The synoptic scale features on 14 February were dominated by the redevelopment of the subtropical high pressure cell following a frontal passage the previous day. Surface pressure increased from a low of 1016 mb on 13 February to over 1026 mb on 14 February as the center of the high moved eastward toward the FASINEX area. Wind speeds gradually decreased from 12-13 ms^{-1} at 0000 UT to 5-6 ms^{-1} at 2400 UT. The wind direction shifted from northwest to northeast, then gradually to southeast by the 2400 UT. Observed swell heights were 7-10 ft. Cloud cover consisted of multilayer altocumulus and cirrus from 0000 UT to 1800 UT, with some stratocumulus reported at 0700 UT. No precipitation was recorded.

Fig. 4.2 shows the 14 February tracks of the Oceanus and the Endeavor. The Oceanus moved west, then south, while the Endeavor followed a nearly rectangular path ending 155 km northwest of the Oceanus.

On 15 February, the subtropical high moved rapidly northeastward, resulting in a sea-level pressure decrease from 1024 mb at 0000 UT to 1015 mb at 1900 UT. Wind direction shifted from southeast to southwest at 0610 UT, marking the passage of the surface ridge, and remained southwesterly until nearly the end of the period. A deepening 500-mb trough and associated surface low pressure system began to affect the area by 1000 UT, increasing the sea-level pressure gradient and causing wind speeds to increase from 6 ms^{-1} to 10-14 ms^{-1}. The cold front associated with the surface low passed the Oceanus at 2330 UT and the Endeavor at 2350 UT. Both ships recorded a 2.2° C decrease in air temperature and a wind shift from southwest to west as the front passed. Cloud cover consisted of multilayer stratus, stratocumulus, and altocumulus. The Endeavor recorded a rain shower commencing at 2359 UT. Early in the day, swell heights decreased to 4-5 ft, then increased to 10 ft at the time of the frontal passage.

The ship tracks for 15 February are shown in Fig. 4.3. The Oceanus moved south, then west, then north. From 2100 UT to 2400 UT she moved west, effectively increasing the speed with which the front approached her. The Endeavor followed a more erratic path and remained in a nearly constant position during the frontal passage.

On 16 February, following the frontal passage, surface pressure increased steadily, reaching 1026 mb by 2400 UT. Wind speeds decreased rapidly to 6.5 ms^{-1} within 4 h of the frontal passage, then remained steady at 6-8 ms^{-1} for the remainder of the day. Wind direction shifted from northwest to northeast as the subtropical high

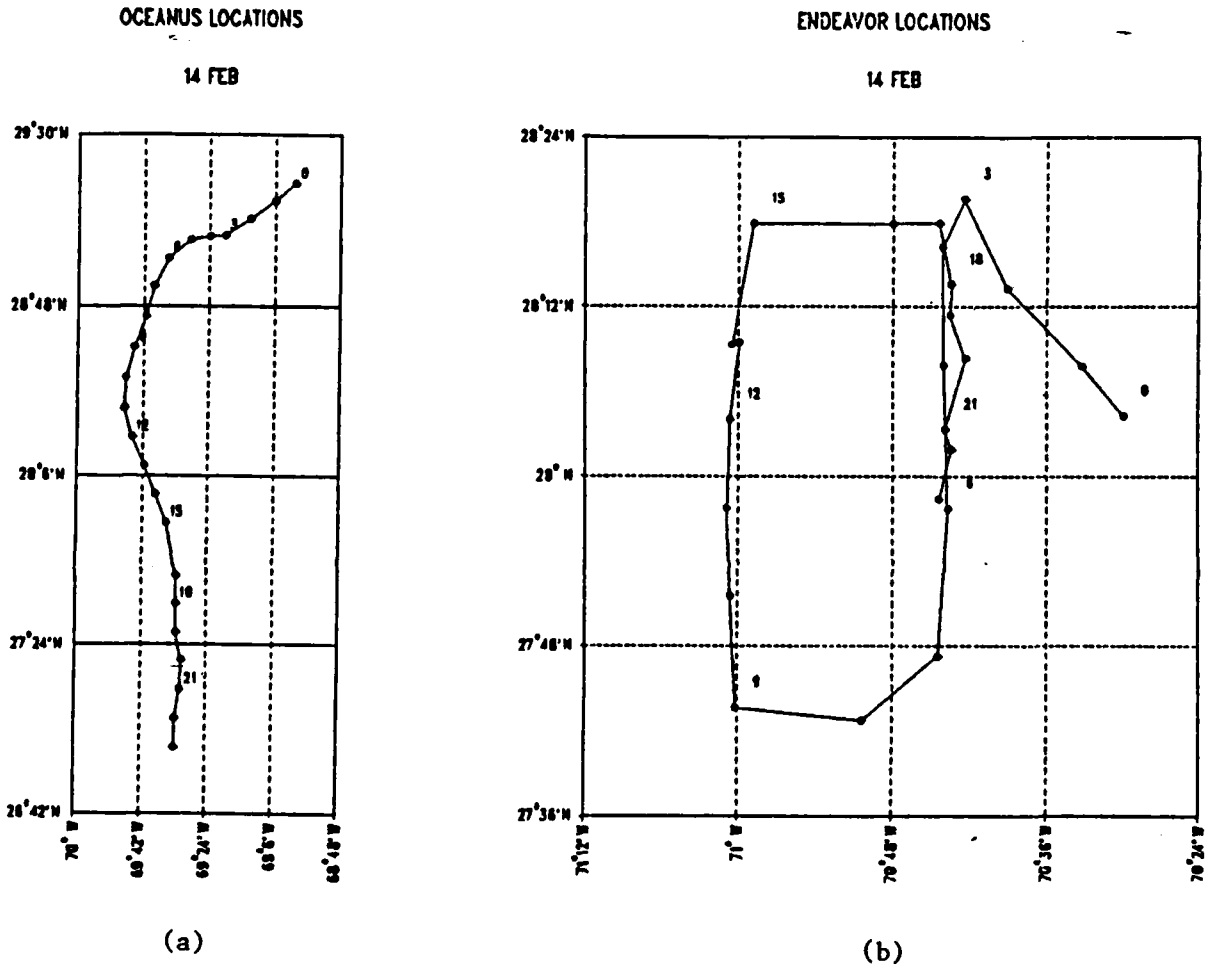

Figure 4.2 Oceanus (a) and Endeavor (b) tracks for 14 February.

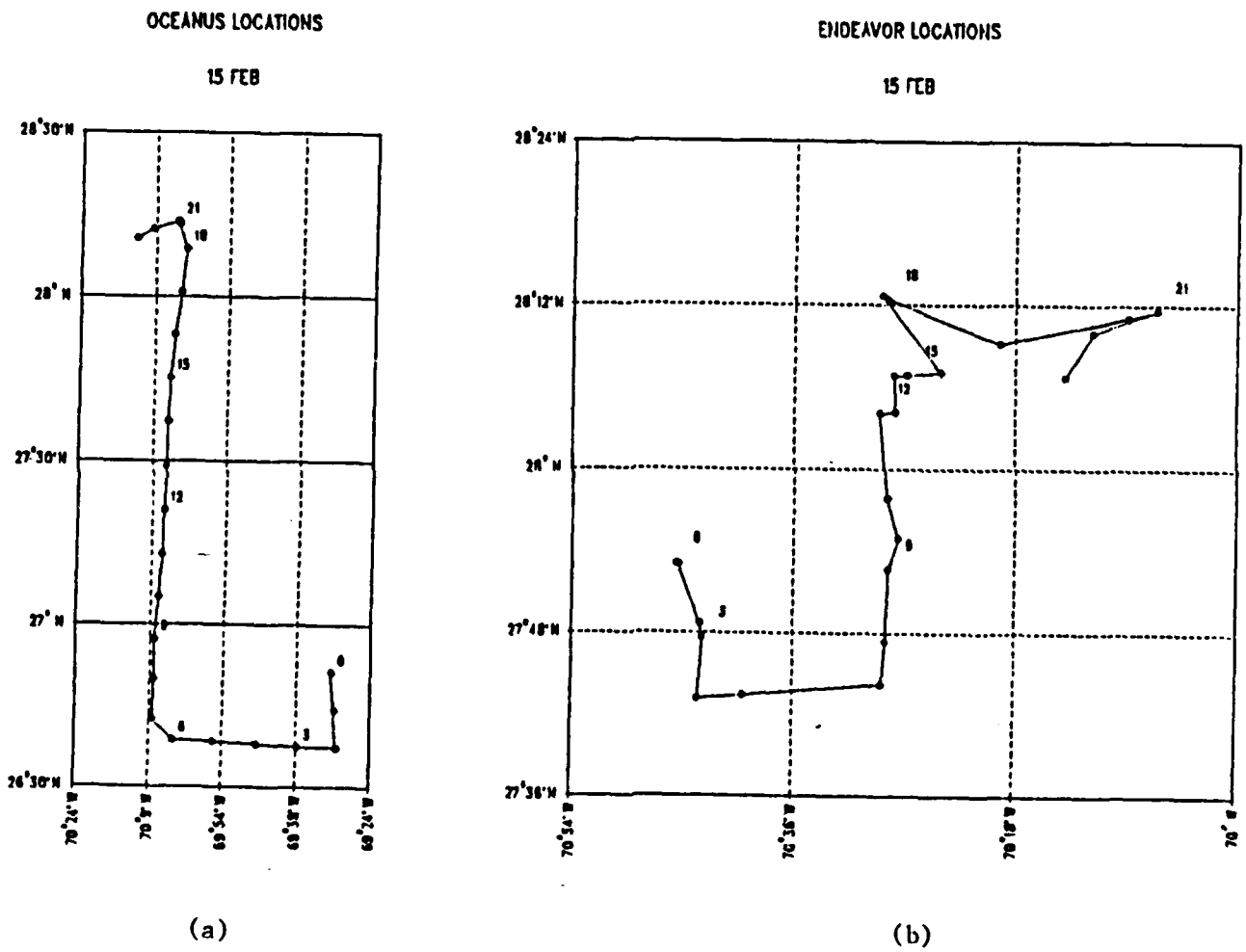

(a) (b)

Figure 4.3 Oceanus (a) and Endeavor (b) tracks for 15 February.

again began to dominate the synoptic-scale pattern. Rainshowers continued though 0100 UT, and cloud cover consisted of low stratus and stratocumulus thoughout the day. Swell heights decreased to 5-6 ft during the day.

The 16 February ship tracks are shown in Fig. 4.4. The Oceanus moved south, remained on station for several hours, then moved northeast, then south again. She remained well south of the center of the high pressure cell. The Endeavor moved west, then north, then south. Her final position was 137 km northwest of the Oceanus.

2. Frontal Cross-sections for the 15 February Frontal Passage

In Fig. 4.5 are frontal cross-sections of the ratio of dissipation to bulk stress for both ships, and the wind-swell direction difference and swell heights for the Endeavor during the 15 February frontal passage. The stress ratio plot shows two peaks prior to the frontal passage. The first stress ratio maximum of 2.3 occurred near 575 km ahead of the front. This peak coincides with a minimum in the wind-swell direction difference, but is accompanied by an increase in swell height from 6 to 7 ft.

The major region of stress enhancement occurred over a distance from 500 km ahead of the front to the front, with a peak stress ratio of 2.6 at 400 km ahead of the front. This location correlates well with a peak in the wind-swell direction difference, which occurred as the swell shifted from southwesterly to westerly, and the winds followed more slowly. This appears to be a case of westerly swell radiating from behind the front. This could have lead to wave convergence and enhanced stress ahead of the front. The wind speed remained nearly constant at 11-13 ms^{-1} during this period, and the increase in swell height occurred after the increase in stress ratio.

Following the frontal passage winds decreased rapidly and swell heights also decreased. These changes were associated with a decrease of the stress ratio to below 1.0 despite an increase in the wind-swell direction difference. The swell height peak occurred approximately 350 km closer to the front than the stress ratio peak, indicating a time lag of approximately 5 h.

C. THE FRONTAL PASSAGE OF 20 FEBRUARY 1986

This front was associated with a developing wave. It moved more slowly (approximately 25 km/h relative to the ships) than the 15 February front, but had nearly the same intensity (2-3° C air temperature decrease). The sea-level pressure maps for this frontal passage are in Fig. 4.6.

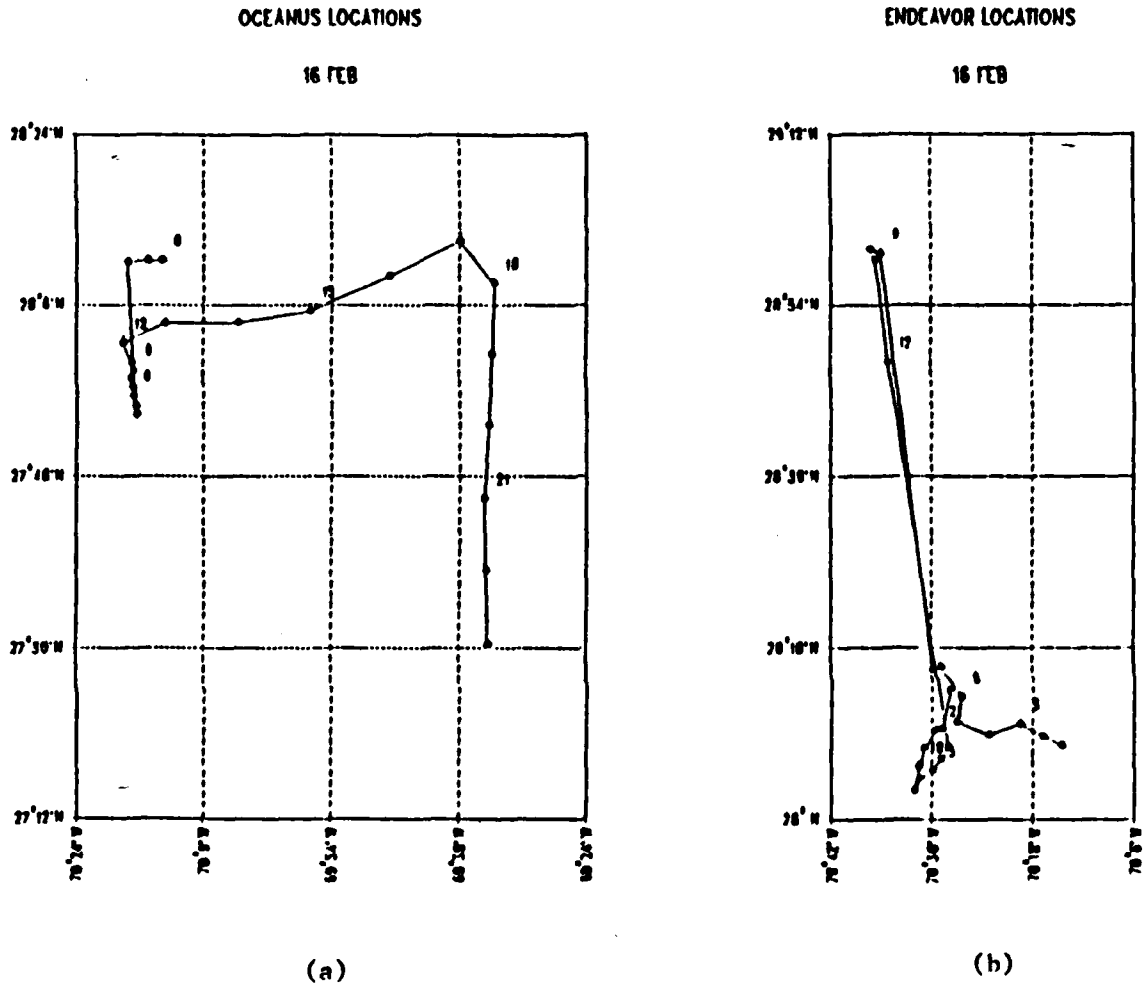

Fig. 4.4 Oceanus (a) and Endeavor (b) tracks for 16 February 1986.

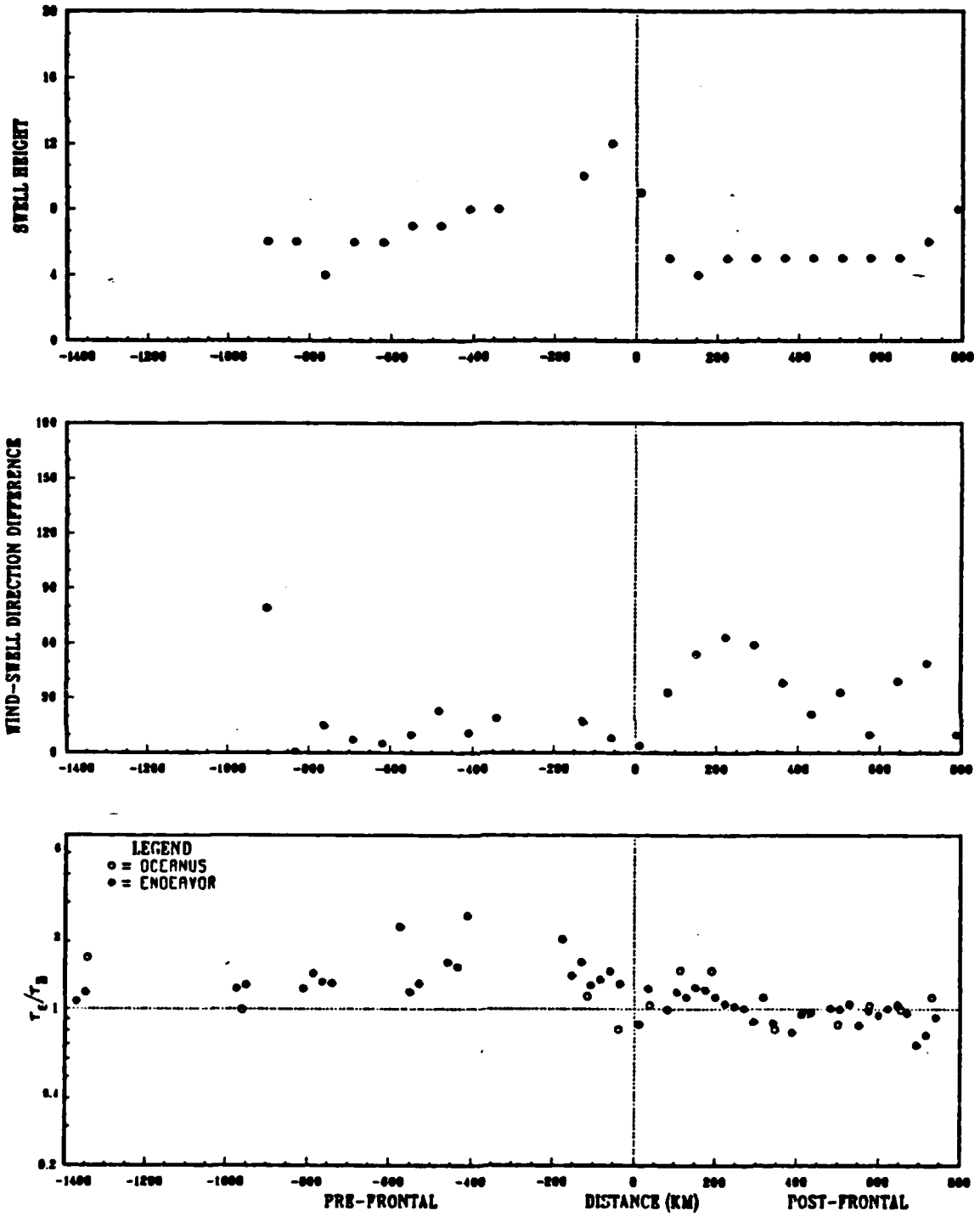

Fig. 4.5 Frontal cross-sections for the frontal passage of 15 February 1986.

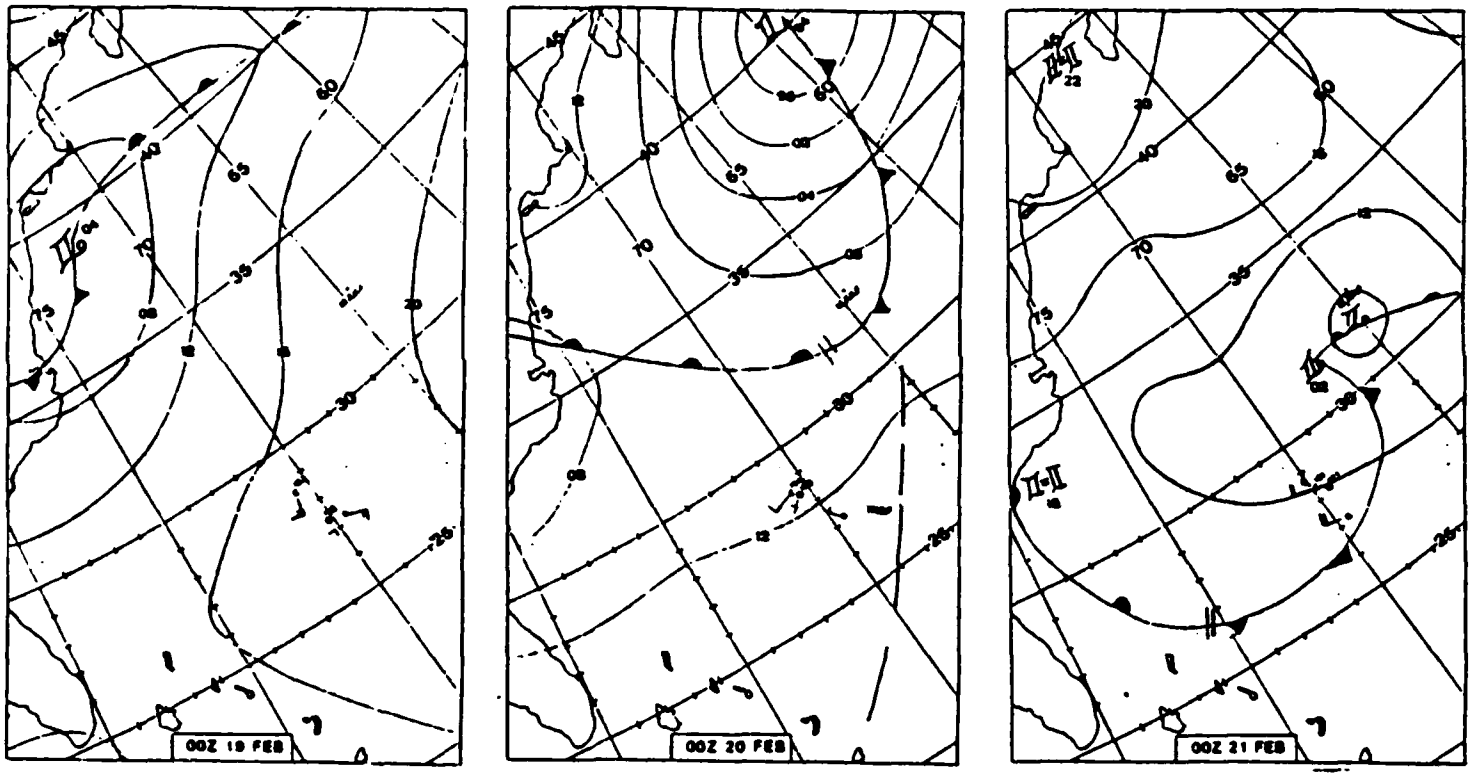

(a) (b) (c)

Fig. 4.6 Sea-level Pressure Maps for 19 Feb (a), 20 Feb (b), 21 Feb (c) 1986.

1. **Synoptic Discussion, 19-21 February**

At 0000 UT 19 February the area remained under the influence of the subtropical high pressure center to the east, with southerly winds of 6-8 ms^{-1}, scattered cloudiness, and 4-ft swells from the south. Winds began to veer to the southwest by 0900 UT as an upper level trough and associated surface low pressure system moved off the U. S. east coast to the north of the area. As the surface low passed to the north, winds continued to veer, and became northwesterly as the surface trough line passed the Endeavor at 1330 UT, and the Oceanus at 1430 UT. After the trough passage, the winds backed slowly, becoming southwesterly by 2400 UT. Wind speeds were steady at 6-8 ms^{-1} thoughout the day, and swell heights constant at 4 ft. Cloud cover increased as the surface low passed, becoming broken to overcast by 1200 UT, and consisted of stratus and altostratus with some cirrus. A rain shower occurred at 0500 UT, and a light rain shower at 1100 UT. Cloudiness decreased, becoming scattered by 2400 UT.

The tracks of the two ships for 19 February are shown in Fig. 4.7. Both ships followed zigzag tracks, with the Oceanus ending northwest of her original position and the Endeavor 33 km southeast of the Oceanus.

During the early portion of 20 February, weak high pressure again dominated the region, sea-level pressures reaching 1015 mb. Winds continued southwesterly at 5-8 ms^{-1}, with swell from the west at 3-5 ft. Scattered cloudiness prevailed. Later in the day, a developing wave moved rapidly off the coast and across the area, resulting in a westerly wind shift and an increase in wind speed to 10-12 ms^{-1}. Cloudiness increased, becoming broken, and rain occurred at 0700 UT. A severe thunderstorm was recorded from 1735-1740 UT. The cold front associated with this system passed the Endeavor at 2115 UT and the Oceanus at 2215 UT. Endeavor experienced a 2° C drop in air temperature, Oceanus a 2.8° C drop. Swell heights remained at 4-6 ft though 2000 UT, increasing to 8-10 ft by 2400 UT as the front passed. Winds shifted to northwesterly 10-12 ms^{-1} following the frontal passage and remained there though 2400 UT.

The ship tracks for 20 February are shown in Fig. 4.8. The Oceanus moved north, then southeast (directly away from the approaching cold front) for 7 h, then remained within a 25-km radius of one station for the remainder of the day. She moved very little as the front passed. The Endeavor, on the other hand, moved southwest, then northeast (essentially paralleling the approaching front), remained on one station for 5 h, then transited south as the front approached.

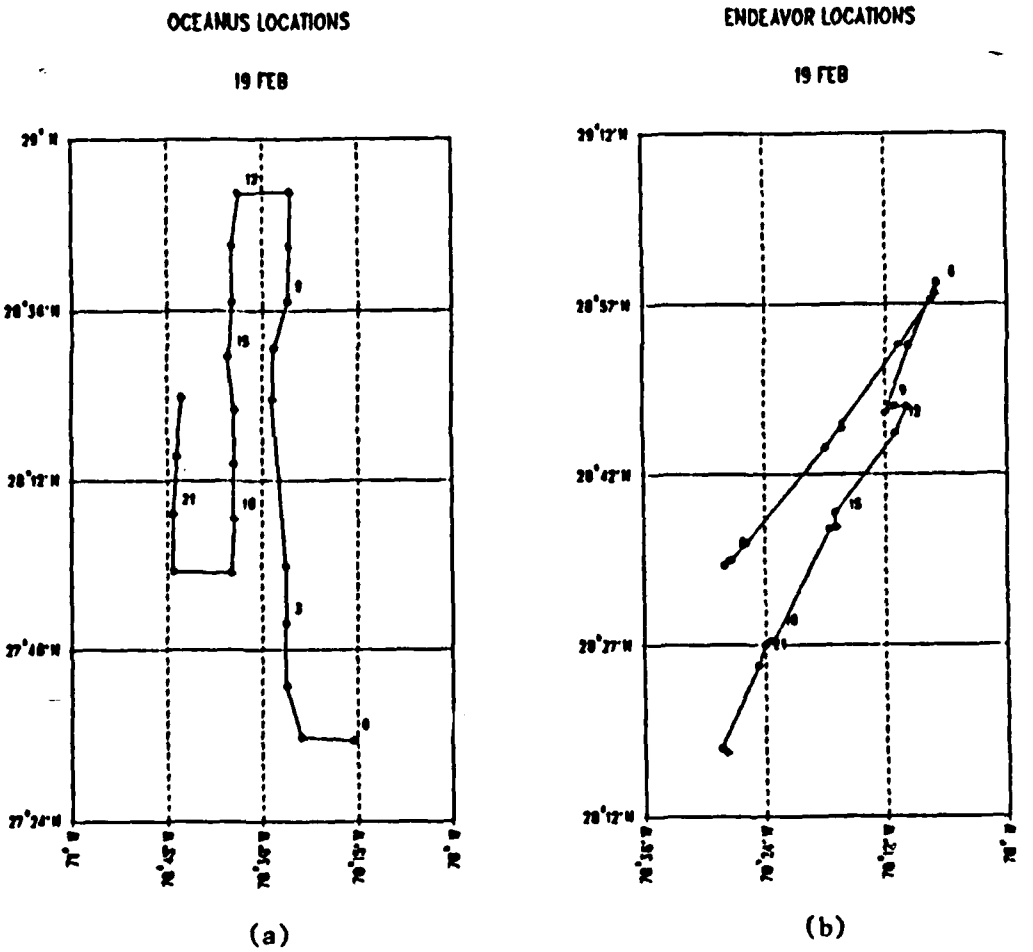

Fig. 4.7 Oceanus (a) and Endeavor (b) tracks for 19 February 1986.

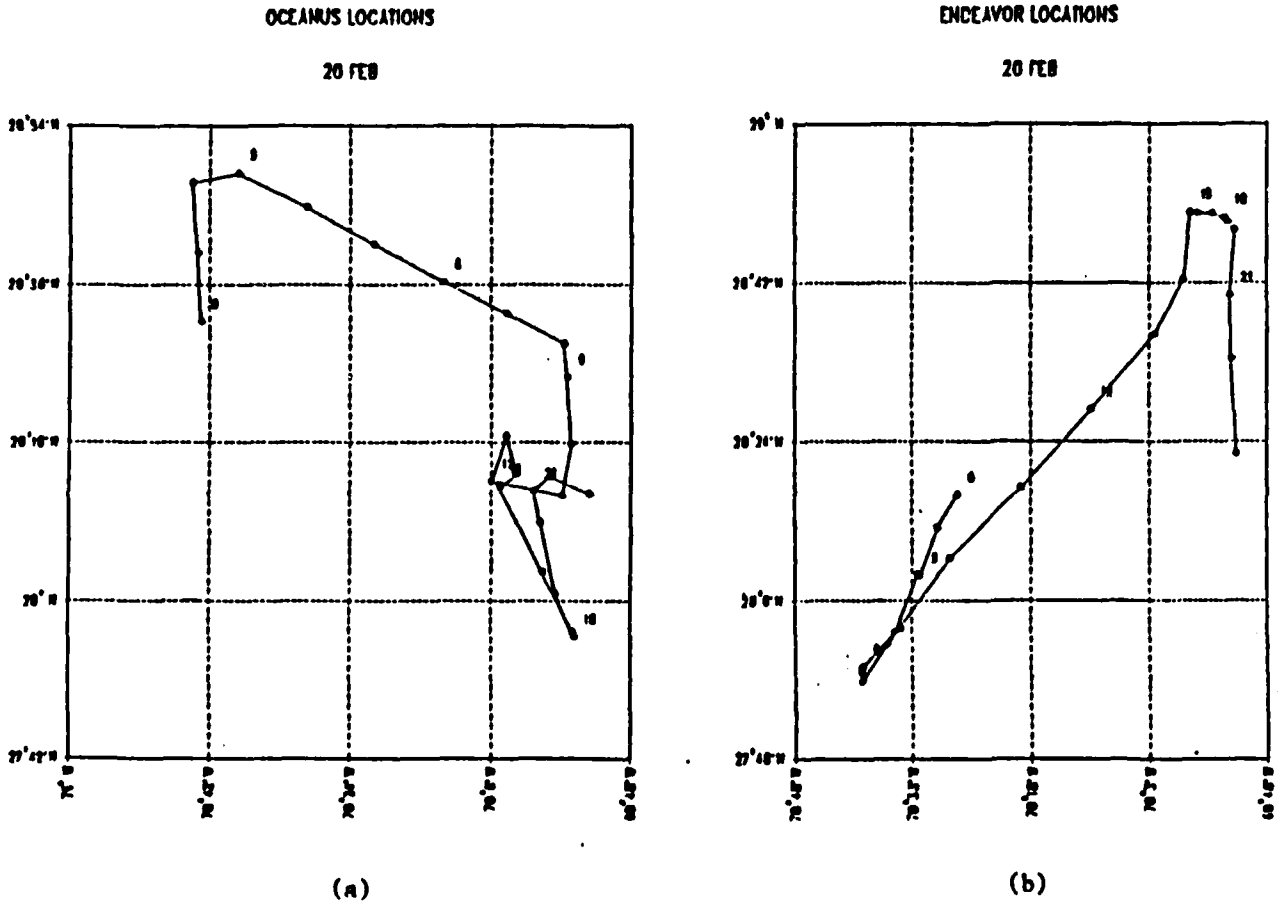

Fig. 4.8 Oceanus (a) and Endeavor (b) tracks for 20 February 1986.

As the upper level trough moved out of the area on 21 February, a weak surface high developed. Wind speeds decreased to 3-5 ms^{-1} by 2400 UT, and the direction shifted from westerly to northeasterly. The swell also became northeasterly, and decreased to 3-5 ft by 2400 UT. Cloudiness decreased, becoming scattered to clear, with only patches of low stratus observed.

During 21 February both ships followed erratic tracks, as shown by Fig. 4.9.

2. **Frontal Cross-sections for the 20 February Frontal Passage**

The frontal cross-sections from both ships for the 20 February frontal passage are shown in Fig. 4.10. The Endeavor had a more complete record following the frontal passage than did the Oceanus.

Two characteristics are apparent in Fig. 4.10. The first is that the variations in the stress ratio correlate to a high degree with those in the wind-swell direction difference. The second is that, as in the previous frontal passage, increases or decreases in swell height occur after the corresponding changes in the stress ratio. The swell height peak occurs approximately 8 h after the stress ratio peak. The major stress enhancement (a peak ratio of 2.3, 150-200 km ahead of the front) appears to be related to radiation of swell from behind the front and the resulting wave convergence. During this period the swell direction shifted from southwest to west, while the wind direction remained southwesterly. The period of decreased stress ratios occurring 400-600 km ahead of the front seems related to the appearance of a southeasterly to south-southeasterly swell train, possibly from a distant storm. Here the swell direction was nearly opposite the wind direction, and may have had the effect of modulating wave breaking and thus decreasing energy transfer into the ocean surface.

The region of enhanced stress ratios approximately 800 km ahead of the front corresponds with the passage of a surface trough, during which the swell direction changed from south to west-southwest over 2 h prior to the wind shift. This is similar to the events occurring with the frontal passage, and suggests that the wave convergence mechanism may also operate prior to the passage of a strong trough. This serves to confirm the observation of pre-trough enhancement made during STREX by Boyle, *et al.* (1987). Again, the swell height peak occurs after the stress ratio peak.

D. THE FRONTAL PASSAGES OF 25 FEBRUARY 1986

On 25 February there was an unusual situation in which two distinct fronts passed though the region in a period of just over eight hours. The first was a slow-

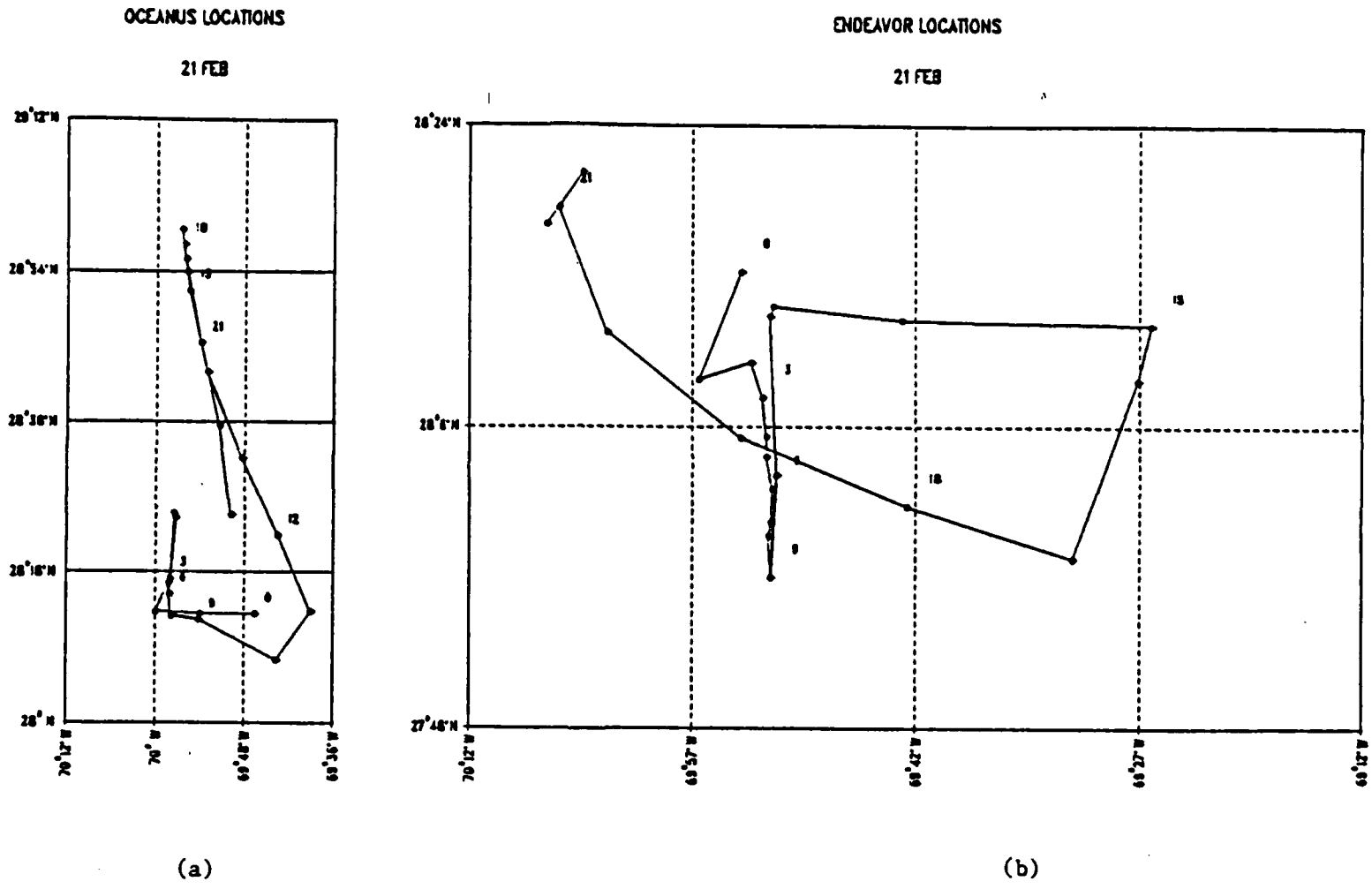

Fig. 4.9 Oceanus (a) and Endeavor (b) tracks for 21 February 1986.

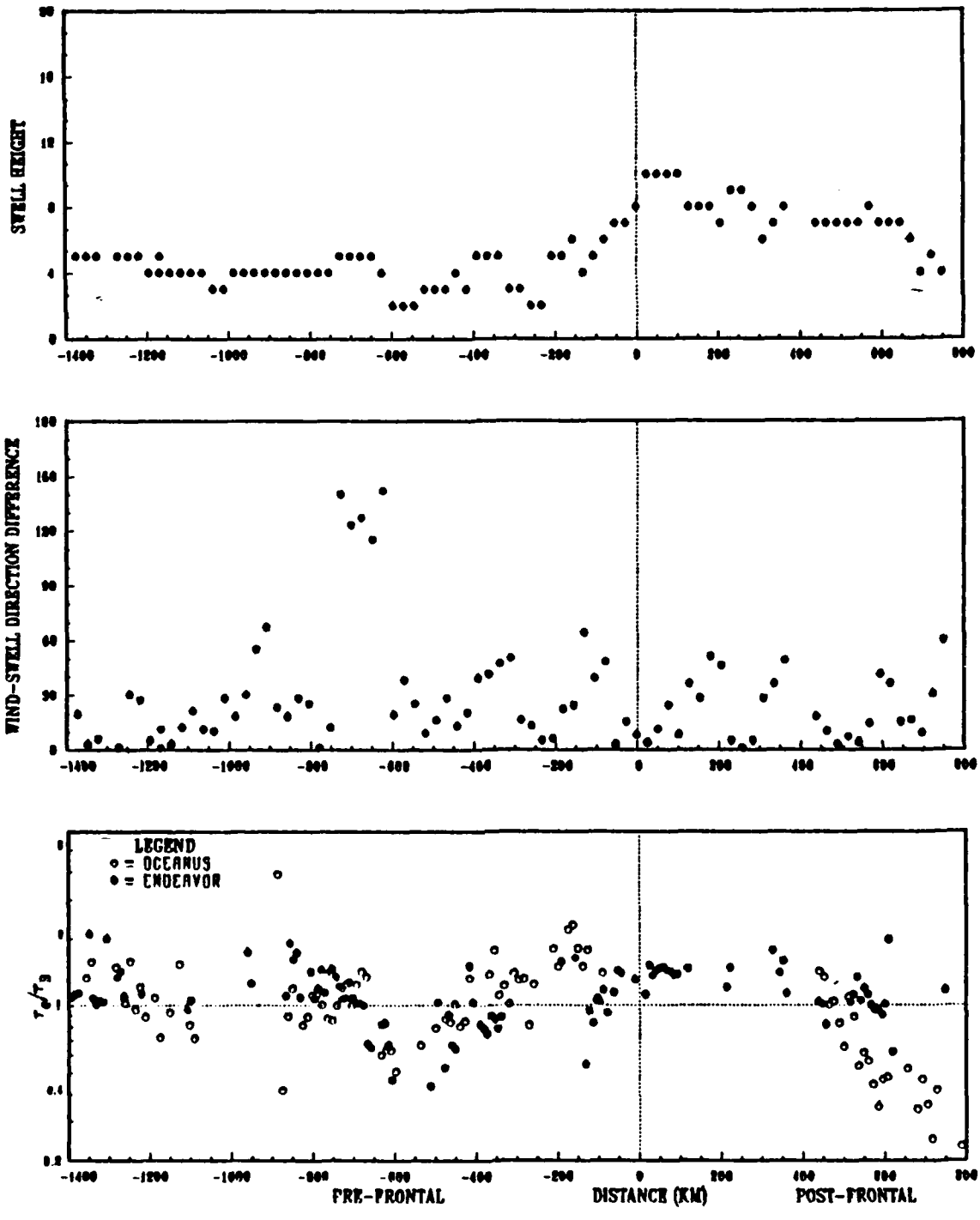

Fig. 4.10 Frontal cross-sections for the frontal passage of 20 February 1986.

moving front of moderate intensity (2.1° C air temperature drop at the Oceanus, 1.8° C drop at the Endeavor), and the second a faster-moving, weak secondary front (0.5° C drop at the Oceanus, 1.0° C at the Endeavor). Stress enhancement was observed to occur with both frontal passages. The sea-level pressure maps for 24-26 February are shown in Fig. 4.11.

1. **Synoptic Discussion, 24-26 February**

A nearly stationary frontal zone with a series of open-wave disturbances was oriented southwest-northeast just west of the FASINEX area on 24 February. A frontal wave located over the southern tip of Florida at 0000 UT propagated rapidly northeast, passing well to the north of the ships and out of the area by 1200 UT. During the period 0000-1200 UT winds were southwesterly at 7-10 ms^{-1} and sea-level pressure was nearly steady at 1015-1016 mb. Swell was from the southwest at 6-8 ft. By 1200 UT a new wave formed on the front just east of Florida. This wave propagated northeast and developed into a 1006 mb low-pressure center located 4° north of the ships by 2400 UT. Surface pressure decreased steadily during the period 1200-2400 UT, reaching 1013 mb by 2400 UT. Winds increased slightly to 8-11 m/s and remained southwesterly, and the swell height increased to 4 ft. Rain occurred at 1430 UT, showers at 1713 UT, and heavy rain at 1851 UT.

The ship tracks for 24 February are shown in Fig. 4.12. The Oceanus remained within approximately 20 km of one station while the Endeavor made two north-south and two east-west transits.

On 25 February the developing cyclone continued on a northeasterly track and continued to deepen, reaching 1002 mb by 0600 UT. During the period 0000-0600 UT the movement of the cold front toward the ships was quite slow, as the track of the low essentially paralleled the southwest-northeast frontal zone. By 0600 UT, however, a secondary front formed behind the first. The resulting complex low system took a more easterly track, bringing the fronts though the region. The first front passed the Endeavor at 1325 UT and the Oceanus at 1530 UT. Wind speed increased to 10-12 ms^{-1} prior to the frontal passage while the direction remained southwesterly. Winds became westerly after the frontal passage and the speed decreased to 8-10 ms^{-1}. Swell increased to 10-12 ft as the front passed, then decreased to 9-10 ft. Swell direction was southwesterly, shifting to westerly after the frontal passage. Surface pressure decreased

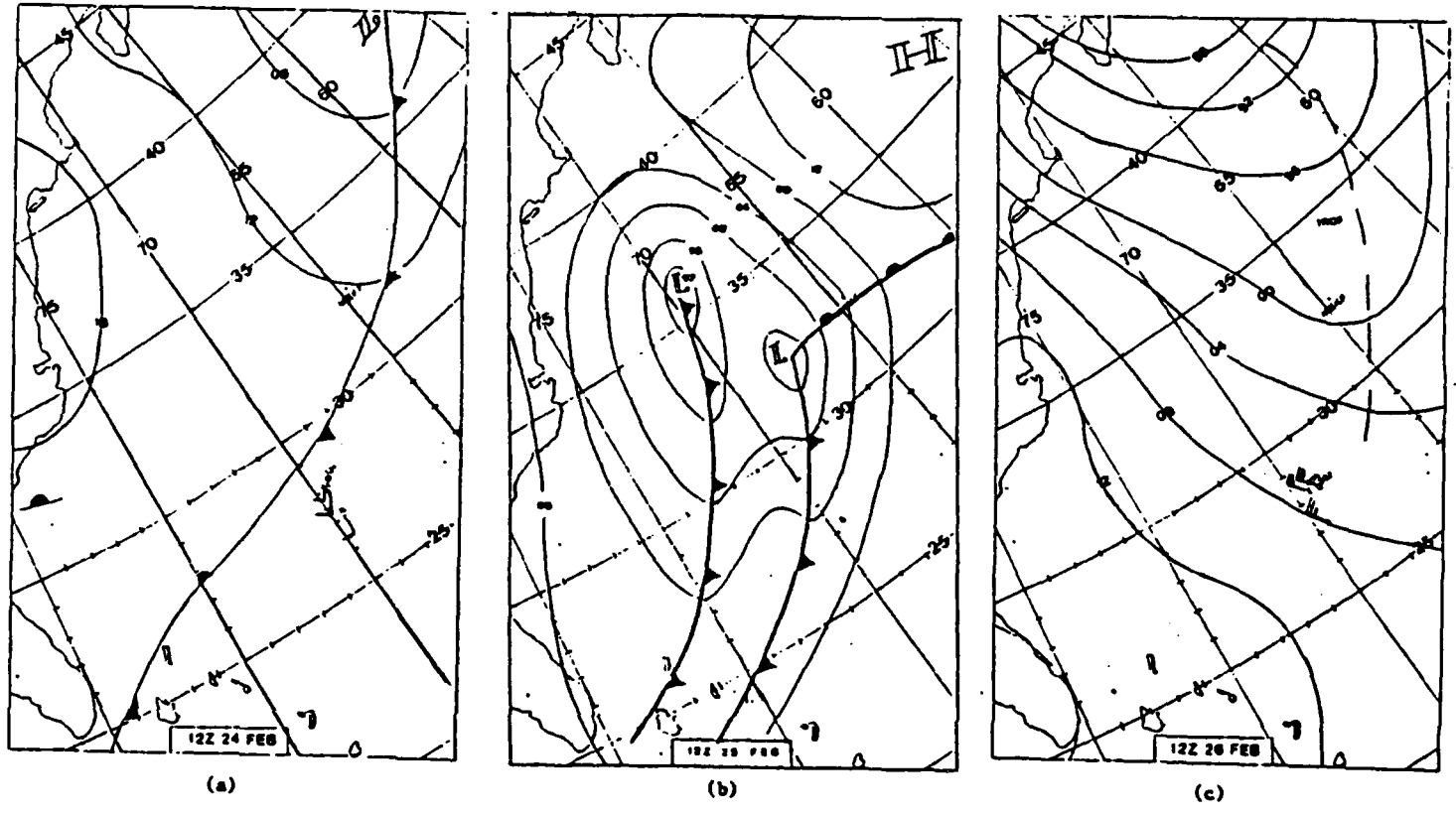

Fig. 4.11 Sea-level Pressure Maps for 24 Feb (a), 25 Feb (b), 26 Feb (c) 1986.

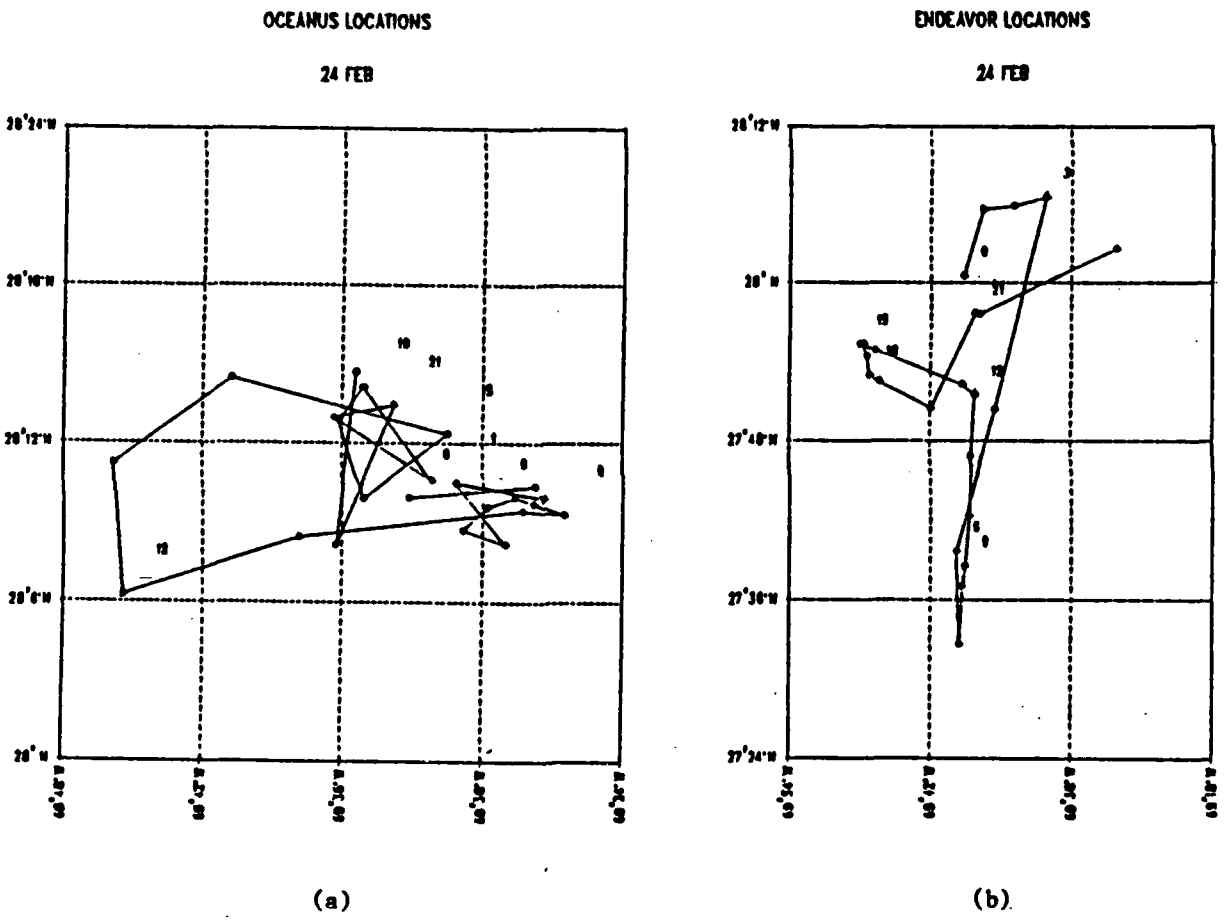

Fig. 4.12 Oceanus (a) and Endeavor (b) tracks for 24 February 1986.

to 1005 mb as the front passed. Rain occurred from 1000-2130 UT, with heavy rain at 2030 UT.

The second front passed the Endeavor at 2155 UT on 25 February and the Oceanus at 2145 UT, accompanied by a shift from westerly to northwesterly winds. Wind speed increased from 8-10 ms^{-1} prior to frontal passage to 11-13 ms^{-1} afterward, and remained there though 2400 UT. Swell direction remained west-northwest at 10 ft. Surface pressure decreased to 1003 mb as the front passed, then increased to 1005 mb by 2400 UT.

During the early portion of 25 February altostratus and cirrus cloudiness was present, with partial clearing at 1300 UT. By 2000 UT a deck of stratus and stratocumulus moved into the area.

The 25 February ship tracks are shown in Fig. 4.13. The Oceanus again remained near one station, while the Endeavor made extensive transits.

Conditions associated with post-frontal periods continued to dominate the area thoughout most of 26 February. Winds were westerly to northwesterly at 10-13 m/s until the influence of the high pressure cell behind the front became evident at around 1630 UT. Wind speeds then decreased to 8-10 ms^{-1} and continued decreasing for the remainder of the day, lowering to 5-6 ms^{-1} by 2400 UT. Swell remained westerly to northwesterly at 11-15 ft until 1800 UT, when it decreased to 8 ft. Cloud cover early in the day consisted of stratus and stratocumulus, with altostratus appearing at 1800 UT. Clearing occurred at 1900 UT as high pressure built behind the front. Heavy rain was observed at 0600 UT.

The ship tracks (Fig. 4.14) were similar for both ships. Because movements were small in the early part of the day, when postfrontal conditions still prevailed, the distances shown in the cross-sections are considered quite accurate for this period.

2. Frontal Cross-sections for the 25 February Frontal Passages

Cross-sections for the first frontal passage on 25 February are shown in Fig. 4.15. The Oceanus stress ratio cross-section is presented because it displays less scatter than the Endeavor cross-section and better illustrates the trend of the data. The Endeavor cross-section is, however, comparable in all essential aspects.

These cross-sections display two similarities with those from the previous cases. The stress ratio variations are, as in the 15 February and 20 February frontal passages, closely correlated with variations in the wind-swell direction difference, and changes in swell height lag the changes in stress ratio.

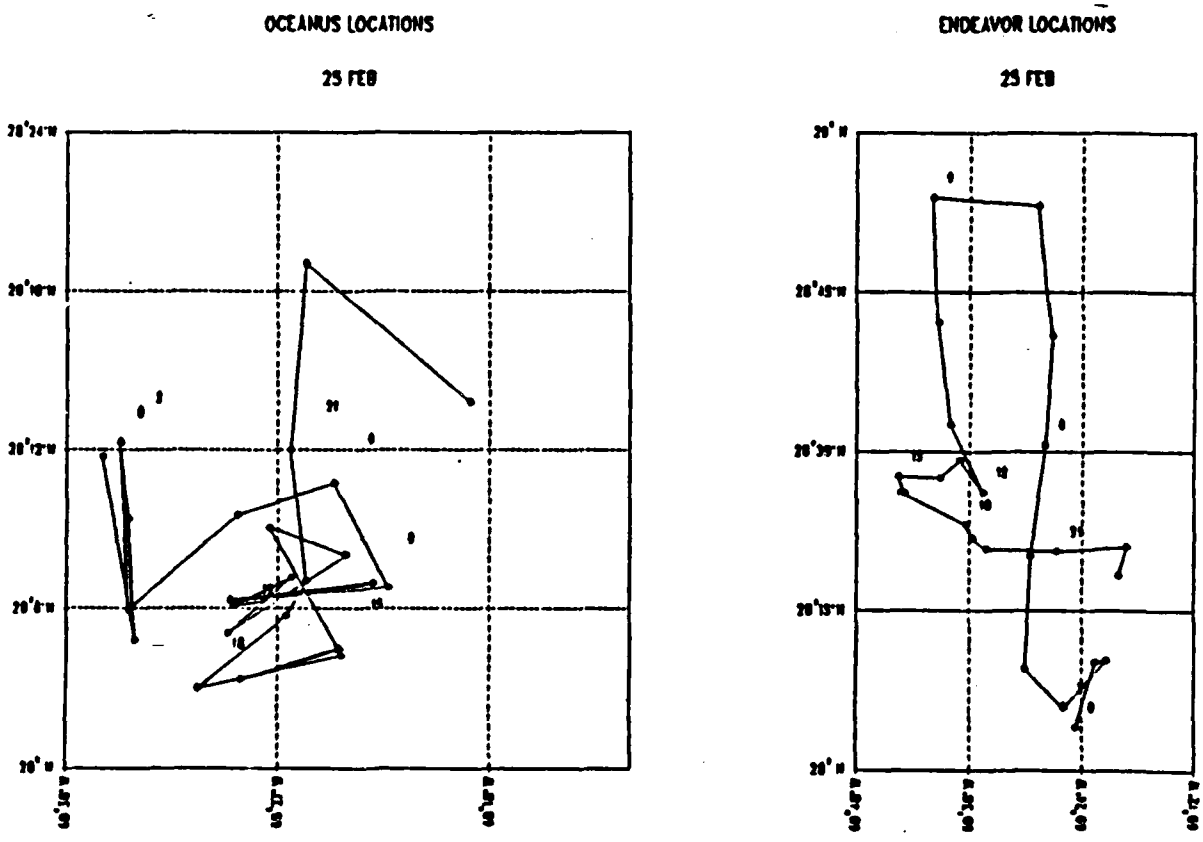

Fig. 4.13 Oceanus (a) and Endeavor (b) tracks for 25 February 1986.

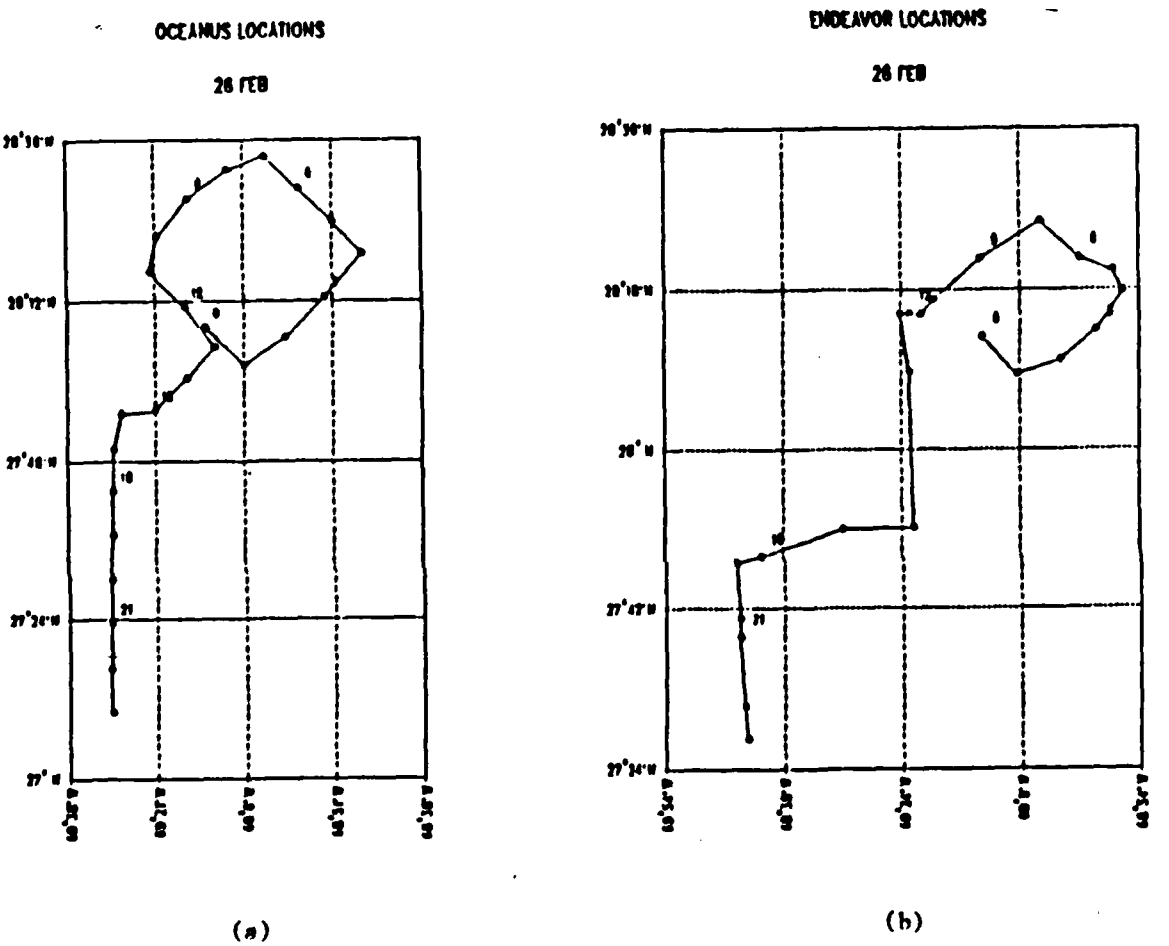

Fig. 4.14 Oceanus (a) and Endeavor (b) tracks for 26 February 1986.

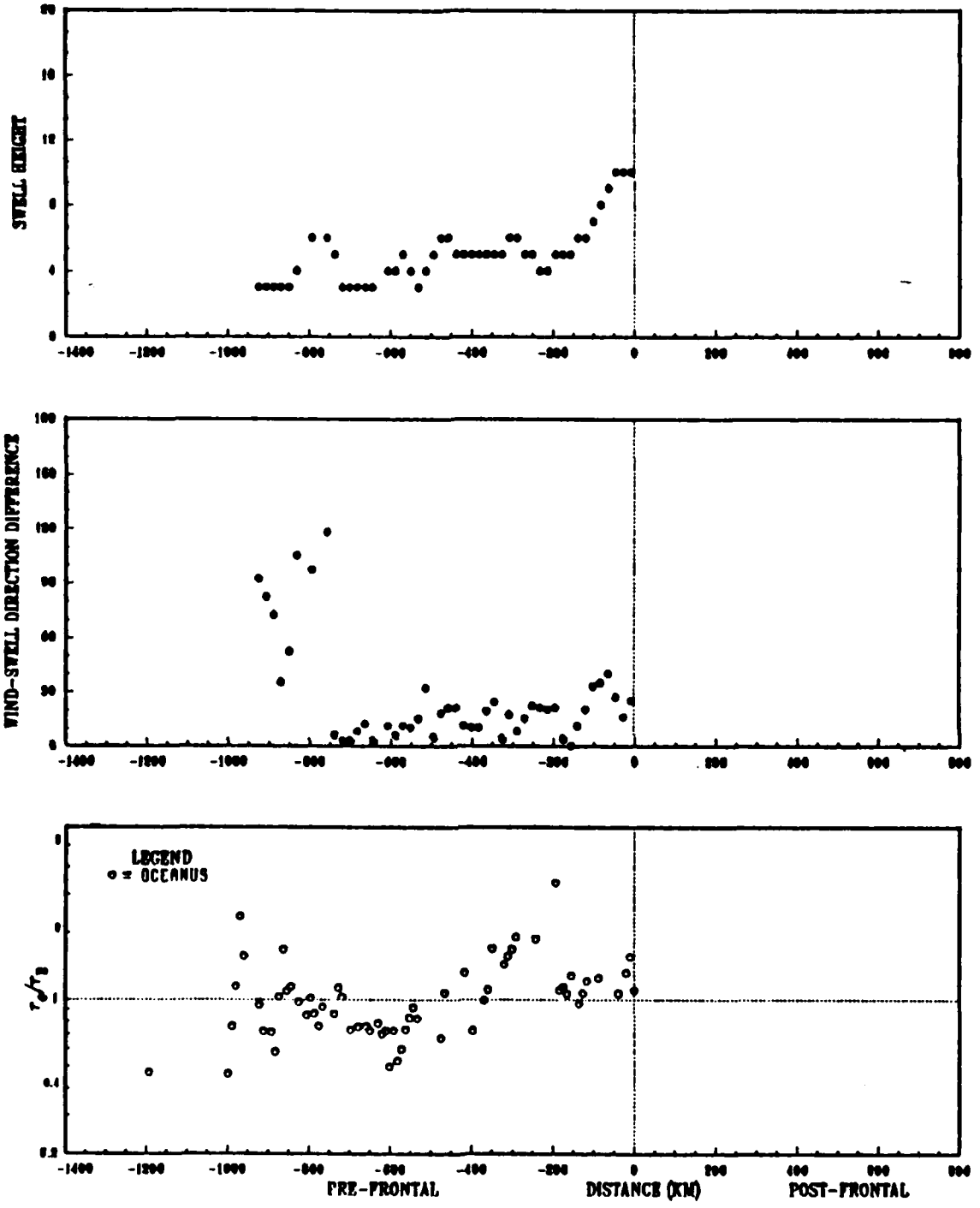

Fig. 4.15 Cross-sections for the first frontal passage on 25 February 1986.

There are two major maxima in the stress ratios, and one distinct minimum. The Endeavor data has its first peak with a ratio of 1.6 near 825 km ahead of the front, while the Oceanus recorded a maximum of 1.6 at 960 km. There are several higher values in the data (i.e. a maximum ratio of 2.7, 860 km ahead of the front in the Endeavor data), but these appear to be anomalous. The peak stress ratios coincide with high values of wind-swell direction difference which occurred as winds shifted from southerly to southwesterly while the swell shifted from easterly to southeasterly.

The second region of stress enhancement, and the one most closely related to the actual frontal passage, began roughly 400 km ahead of the front. The peak stress ratio values were 3.4 at 190 km in the Oceanus data, and 3.6 at 190 km in the the Endeavor data. Again, this peak is correlated with an increase in the wind-swell direction difference, as the swell shifted from the south to the southwest and then the south-southwest while winds fluctuated between southerly and southwesterly. As with the 15 and 20 February frontal passages, significant increases in swell height occurred well after the stress enhancement became evident, and the swell height peak occurred nearly 7 h after the stress ratio peak. The evidence again suggests that the stress enhancement was related to radiation of swell though the front.

The stress ratio minimum occurring between these two peaks coincides with minima in both the wind-swell direction difference and the swell height.

The second frontal passage of 25 February displayed somewhat different patterns because it followed so closely after the first. In this case, illustrated in Fig. 4.16, there was stress enhancement ahead of the front, as before, but with a drop in values to near 1.0 near the frontal passage. There was, however, a strong region of enhancement centered about 400 km behind the front. The stress data in the figure are from both ships; the Oceanus data was missing during the first peak period but the Endeavor data clearly shows a peak before the frontal passage.

The maximum stress ratio encountered in the first peak was 1.4, 200 km ahead of the front. The high stress ratios in this region appear to be related to the confused seas generated by the first frontal passage, and decreased as the second front approached despite an increase in the wind-swell direction difference. As the front passed, a strong (circa 50°) wind shift occurred. The swell field responded more slowly and did not become northwesterly until approxiamately 5 h after the frontal passage. The stress data are missing for this region, however, so it is not possible to determine whether any stress ratio changes were related to these events.

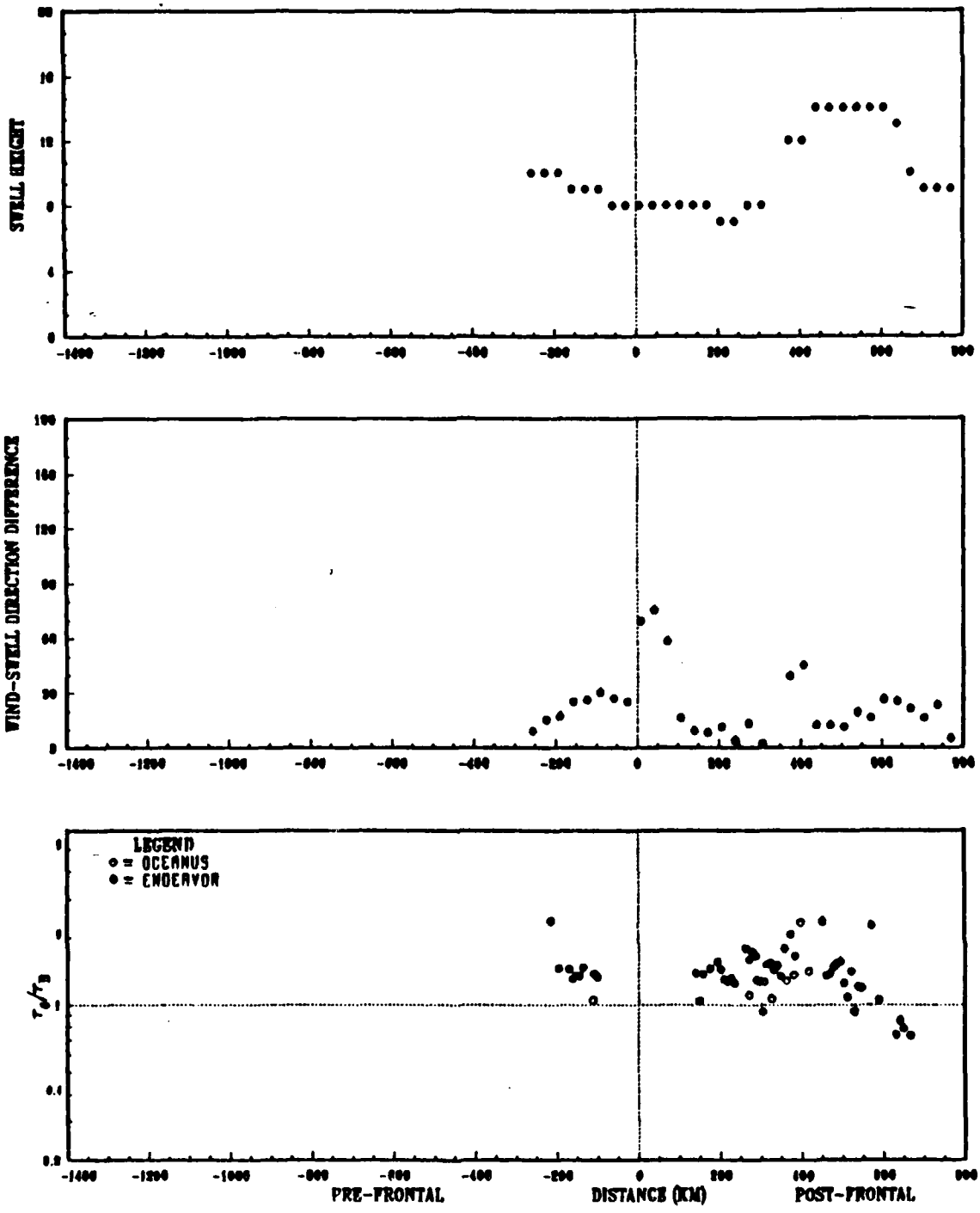

Fig. 4.16 Cross-sections for the second frontal passage of 25 February 1986.

After the frontal passage, stress ratios rose again, reaching a peak value of 2.3 at 400-450 km behind the front. This corresponds to an increase in wind-swell direction difference occurring as the wind direction shifted from west to northwest before the same shift occurred in the swell direction. Again, the swell height peak occurred after the stress ratio peak. In this case, the lag is approximately 1 h.

E. THE FRONTAL PASSAGE OF 2 MARCH 1986

The synoptic-scale pattern associated with this frontal passage was similar to that of the first front on 25 February. A wave cyclone developed along a southwest-northeast oriented frontal zone, then moved northeast along the front. This surface low, however, moved and developed more rapidly than the 25 February low, and had begun to occlude by the time the front passed the ships. No secondary low was present in this case. The synoptic maps for this frontal passage are shown in Fig. 4.17.

1. Synoptic Discussion, 1-3 March

At 0600 UT 1 March the developing cyclone was analyzed as a weak (1008 mb) open wave located roughly 600 km west-northwest of the ships. For the next 6 h it remained ssentially stationary, decpening to 1005 mb, then it began moving to the northeast. By 1800 UT it was located 450 km northwest of the ships, and had a central pressure of 996 mb. Surface pressures in the FASINEX area decreased steadily thoughout the day, from 1013.7 mb at 0000 UT to 1114.7 mb at 2400 UT. Winds began southeasterly at 7-10 ms^{-1} and gradually increased in speed to 16-20 ms^{-1} and shifted to the southwest. Swell was from the south to southeast at 8-11 ft until 1200 UT, then increased to 11-13 ft. By 2000 UT the swell direction had shifted to the southwest. Cloud cover progressed from scattered cumulus and stratocumulus early in the day to broken stratus and fractostratus by 2400 UT. A heavy rain shower was recorded at 1900 UT.

The Oceanus and the Endeavor both made extensive transits during this period (Fig. 4.18).

On 2 March the surface low became occluded and continued to move northeastward. The cold front passed the Endeavor at 0005 UT and the Oceanus at 0030 UT. The Endeavor experienced a 2.3° C air temperature decrease, the Oceanus a 1.3° C decrease, and both ships recorded a westerly wind shift of about 20°. No precipitation was recorded. Winds remained southwesterly at 16-20 m/s until 1500 UT, then began to shift westerly and decrease in speed, falling to 9-12 ms^{-1} by 2400 UT. Swell reached a maximum of 16 ft at 0800 UT, then decreased to 11 ft by 2400 UT.

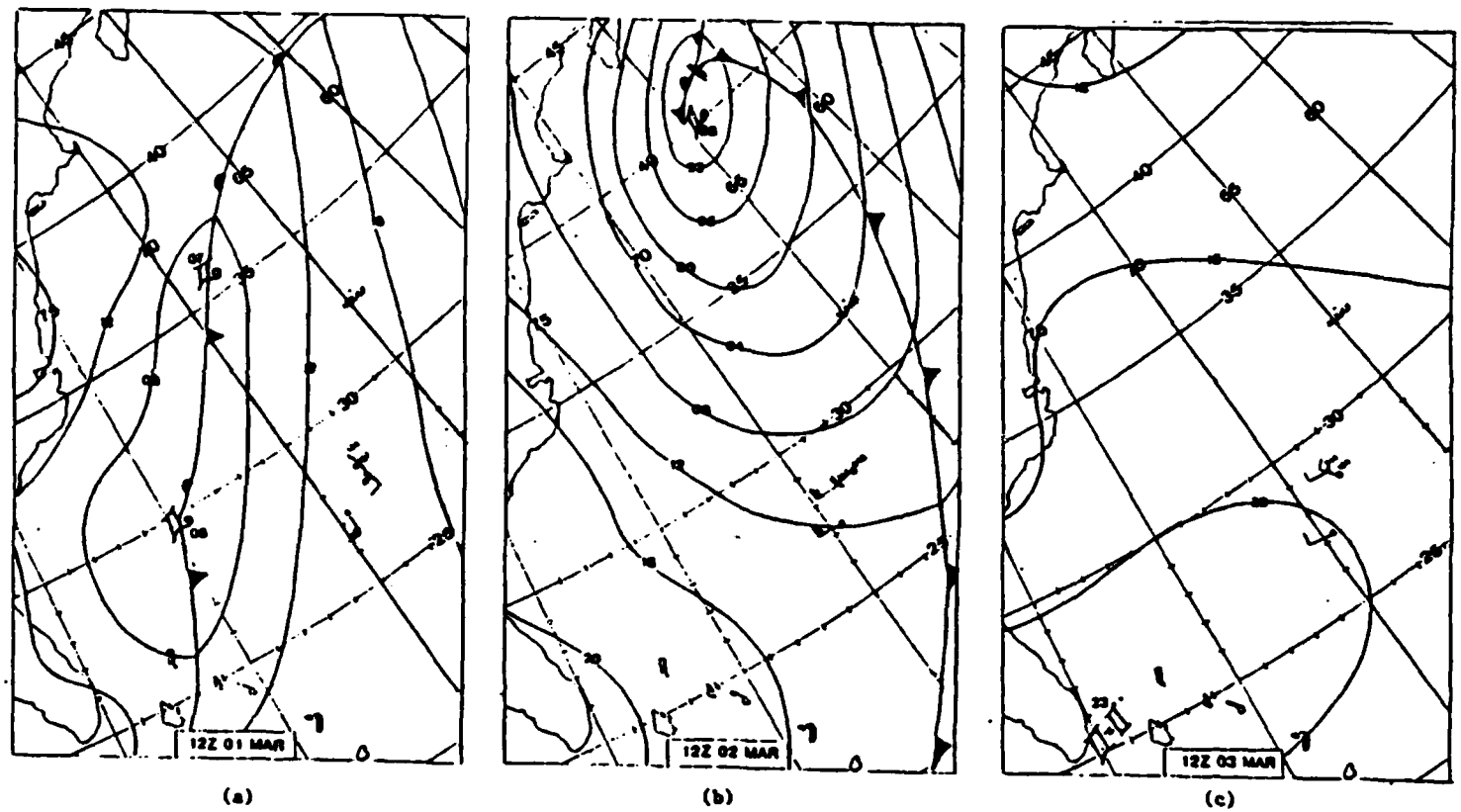

Fig. 4.17 Sea-level Pressure Maps for 1 Mar (a), 2 Mar (b), 3 Mar (c) 1986.

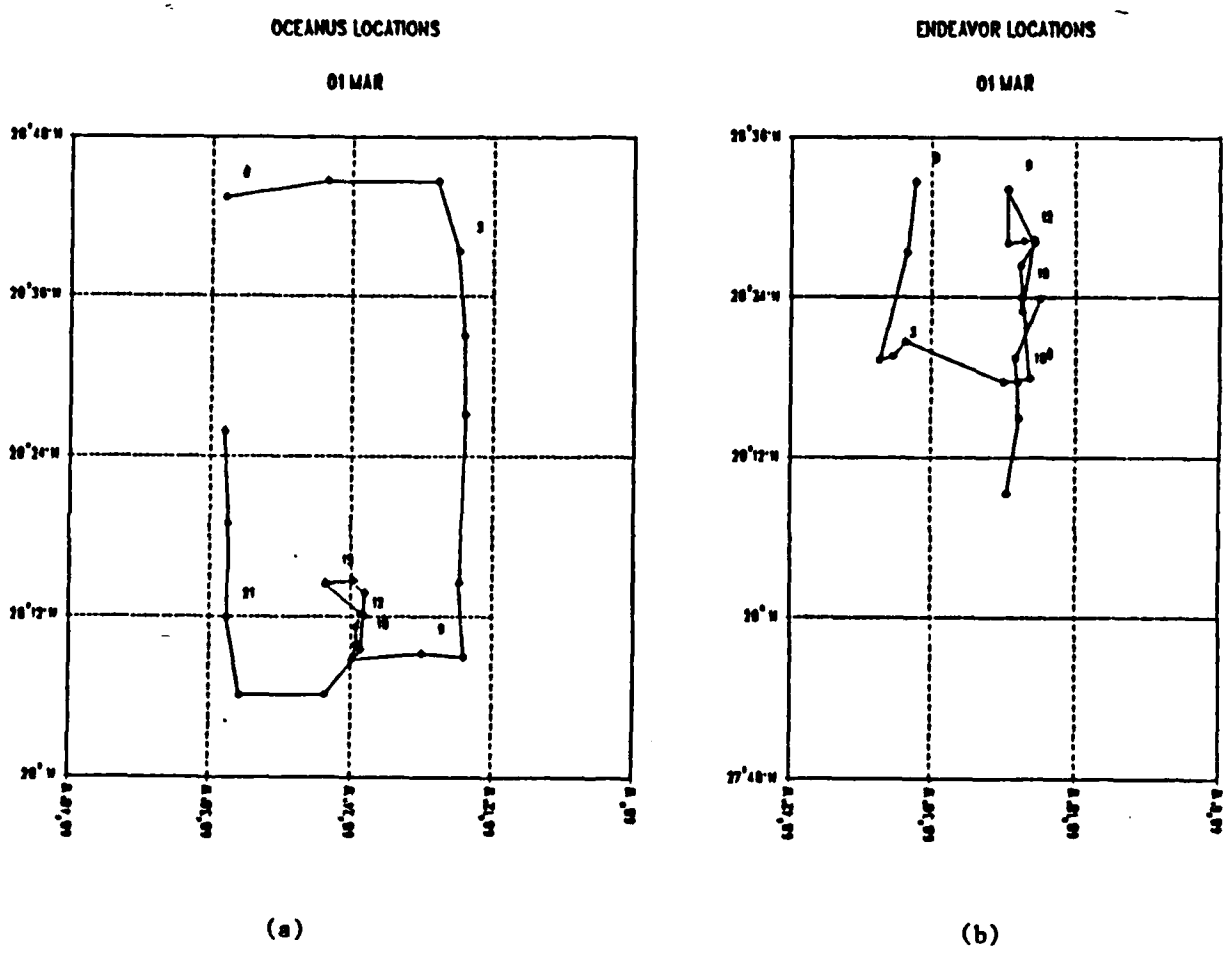

(a) (b)

Fig. 4.18 Oceanus (a) and Endeavor (b) tracks for 1 March 1986.

Swell direction changed steadily from southwest to northwest during the day. Cloud cover was primarily broken altostratus and stratus.

During this period, as shown in Fig. 4.19, the Endeavor remained nearly on one station while the front passed, then made a steady west-northwesterly transit away from the front. The Oceanus, meanwhile, followed a rectangular track. The cross-sections from the two ships show no significant differences related to the ship tracks.

On 3 March the sea-level pressure continued to increase, from 1014 mb at 0000 UT to 1020 mb at 2400 UT, as a surface high pressure center developed to the southwest of the area. Winds remained northwesterly, and decreased from 9-12 ms^{-1} to 3-4 ms^{-1} by the end of the day. Swell heights decreased rapidly to 3-5 ft and swell direction remained northwesterly. The sky became clear, and by 2400 UT 3 March cloud cover consisted of widely scattered altostratus.

The Endeavor transited east, then north, while the Oceanus again followed a rectangular path (Fig. 4.20).

2. **Frontal Cross-sections for the Frontal Passage of 2 March**

The 2 March frontal cross-sections from both ships are shown in Fig. 4.21. The Oceanus data are much less complete, but have both values and trends similar with the Endeavor data.

The stress ratio cross-section for this frontal passage is atypical because it contains two very pronounced minima, centered near 1000 km and 400 km ahead of the front. Both ships' records show stress ratios of 0.5 or below from 1200 km to 950 km ahead of the front, with minima below 0.4 at 1080 km, and ratios below 0.4 from 500 to 385 km, with a minimum of 0.3 at 420 km. The first minimum coincided with a period of significant convective activity, as cumulus and then cumulonimbus cloudiness was noted by the bridge observer, and a heavy rainshower occurred when the front was 1050 km away. The bridge observer reported confused seas during this period, with swell shifting from southwesterly to westerly and decreasing from 10 ft to 7 ft. By 1700 UT on 28 February, two swell trains were apparent, one from the northwest at 9 ft, another from the south-southwest at 6 ft. The northwesterly swell passed out of the area by 2100 UT and seas became south-southwesterly at 8 ft. Winds during this entire period were south-southwesterly at 6-8 ms^{-1}. As for the 20 February case, it appears that this minimum is related to propagation though the area of a train of swell whose direction was nearly opposite the wind direction. In this case, however, the swell was generated by nearby thunderstorms rather than a distant storm. Swell

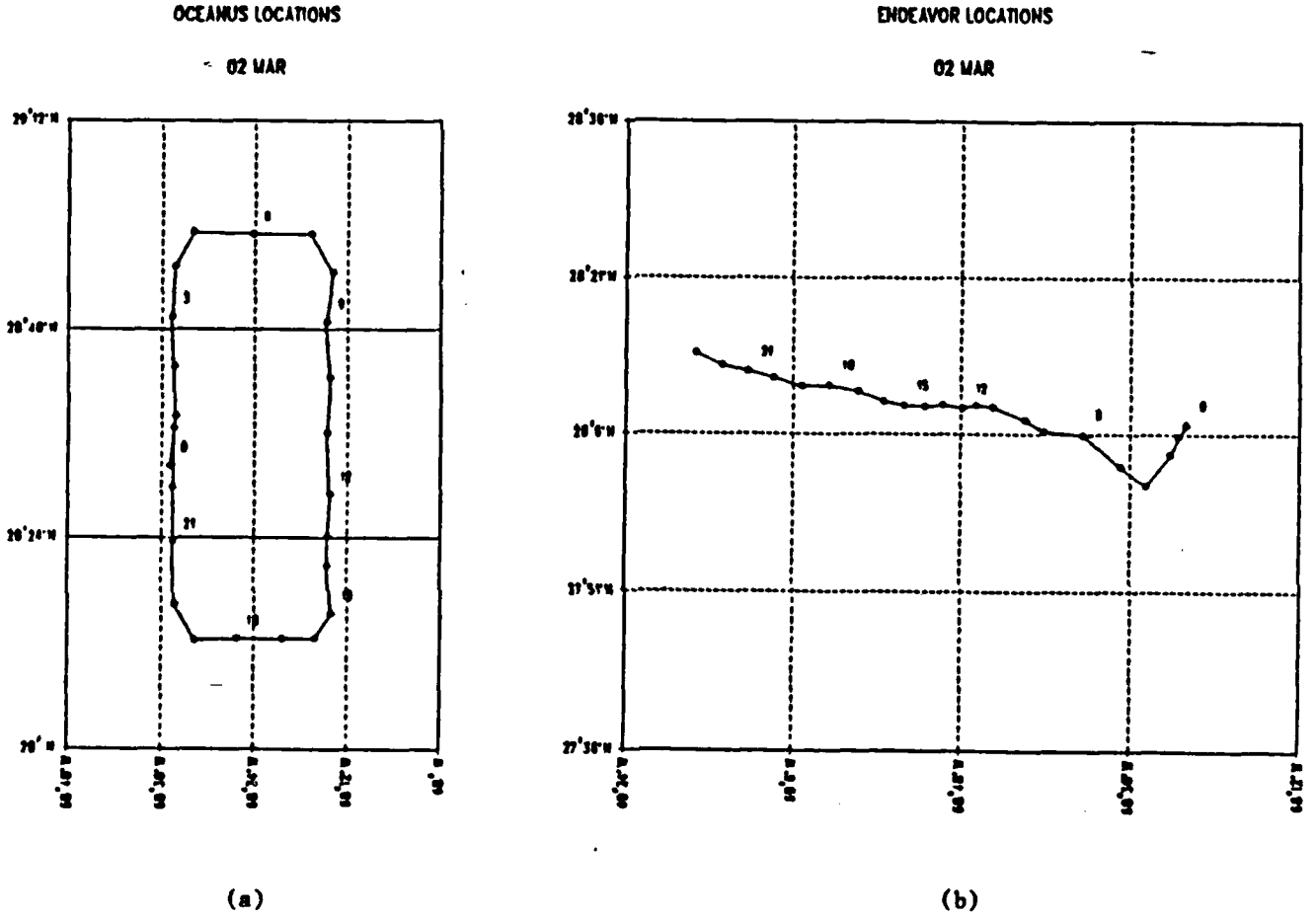

Fig. 4.19 Oceanus (a) and Endeavor (b) tracks for 2 March 1986.

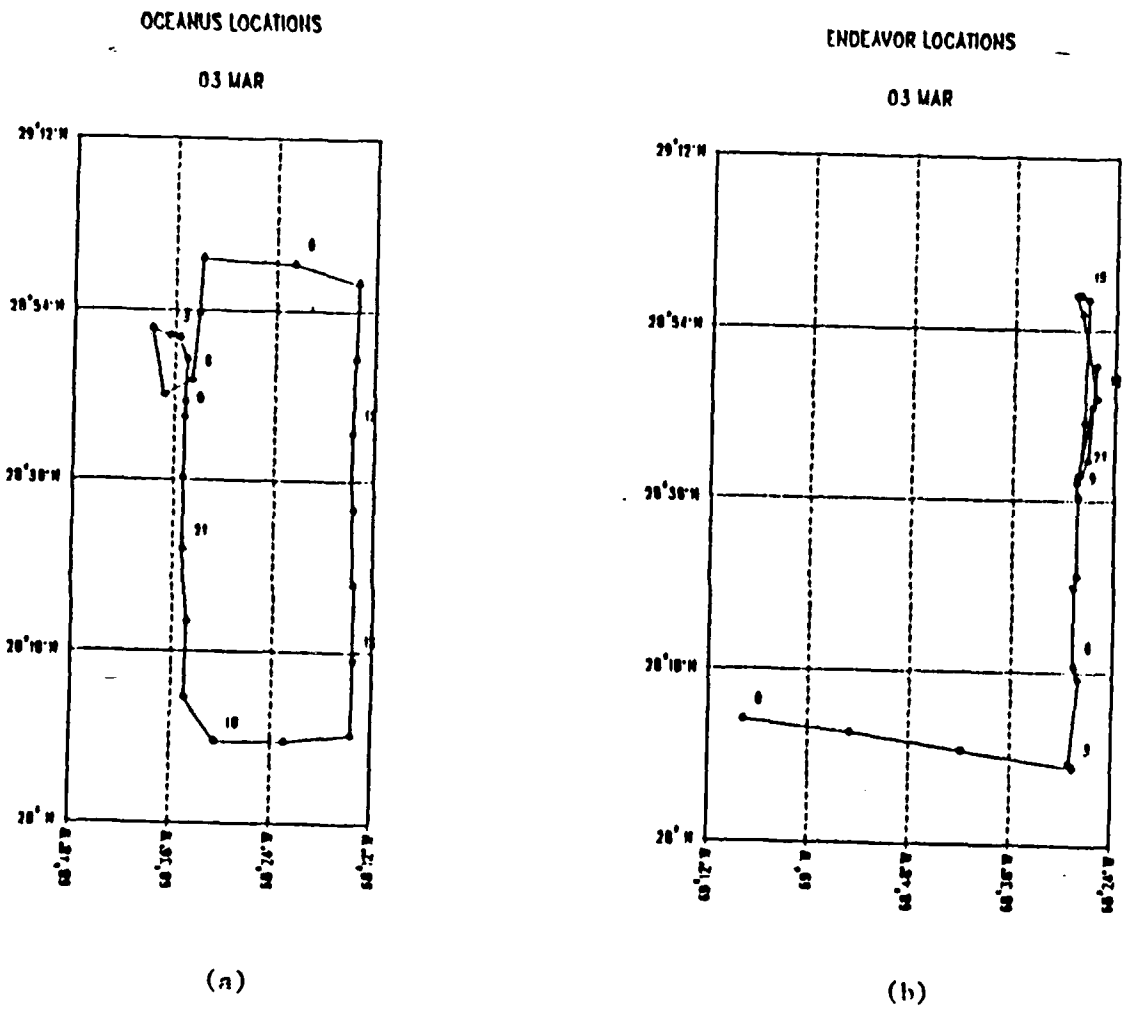

(a) (b)

Fig. 4.20 Oceanus (a) and Endeavor (b) tracks for 3 March 1986.

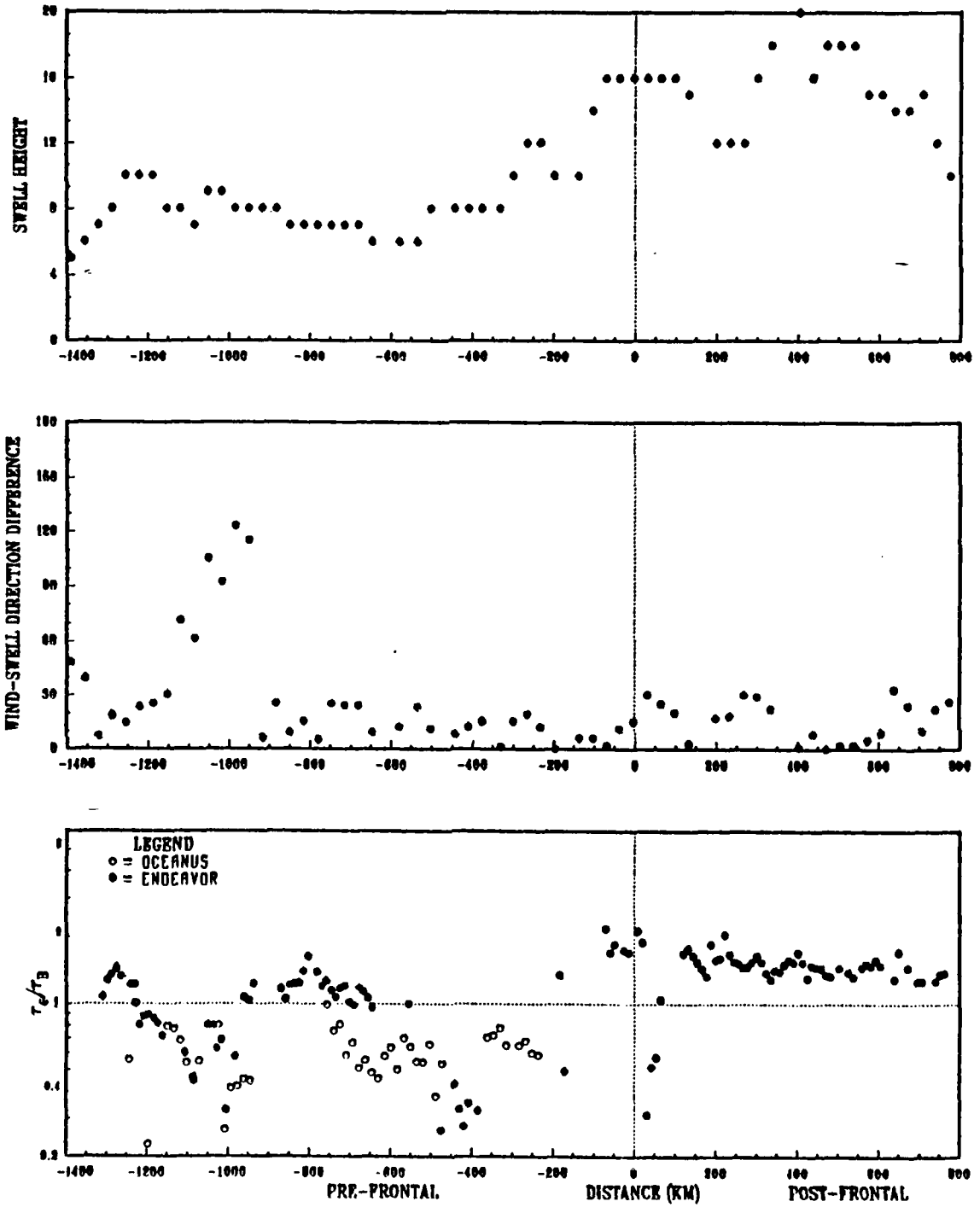

Fig. 4.21 Frontal cross-sections for the frontal passage of 2 March 1986.

propagating nearly opposite the prevailing wind apparently modulated the energy transfer from the atmosphere to the ocean.

The second minimum occurred when both the wind and swell were from the south-southwest and increasing in magnitude. It is difficult to explain this decrease in stress ratios, but its occurrence is supported by the data from both ships.

A region of stress enhancement is evident from approximately 200 km ahead of the front to 600 km behind the front. A stress ratio maximum of 2.1 occurs 70 km before and 10 km after the frontal passage. In this case, the wind-swell direction difference remained low, as both wind and swell were from southerly to south-southwesterly directions. Wind speeds were relatively high thoughout the period (12-16 ms^{-1}, with occasional drops to 10 ms^{-1}), and swell heights decreased to 10 ft, then increased to 16 ft as the front passed. The stress enhancement with this frontal passage appears to be most closely related to the increase in swell height. There is no evidence of swell radiation from behind the front during this episode. It is noted, however, that the stress enhancement is less than in most of the other cases.

F. THE FRONTAL PASSAGE OF 5 MARCH 1986

The front which transited the FASINEX area on 5 March was associated with a complex surface low pressure system which stalled west of the FASINEX area for a day, then moved rapidly though the region. Surface weather maps for the 4-6 March period are shown in Fig. 4.22.

1. Synoptic Discussion, 4-6 March

On 4 March a southwest-northeast oriented front was located northwest of the FASINEX area. A weak wave developed along this front and moved northeast and out of the area. By 1800 UT a small low pressure area moved off the coast and began to approach the frontal zone. Thoughout the day winds remained light (less than 6 ms^{-1}) and southwesterly, and sea-level pressure stayed nearly steady at 1019-1020 mb. Cloud cover consisted of low to mid-level stratus and altostratus, with cirrus appearing at 1830 UT. No precipitation was recorded. Swell was southwesterly at 4-6 ft thoughout the day.

The ship tracks for 4 March are shown in Fig. 4.23. Because the front was essentially stationary and located some distance from the ships, the tracks should have little effect on the accuracy of the cross-section distances.

The approach of the surface low was associated with the formation of a new wave along the frontal zone on 5 March. This wave moved rapidly north-northeast,

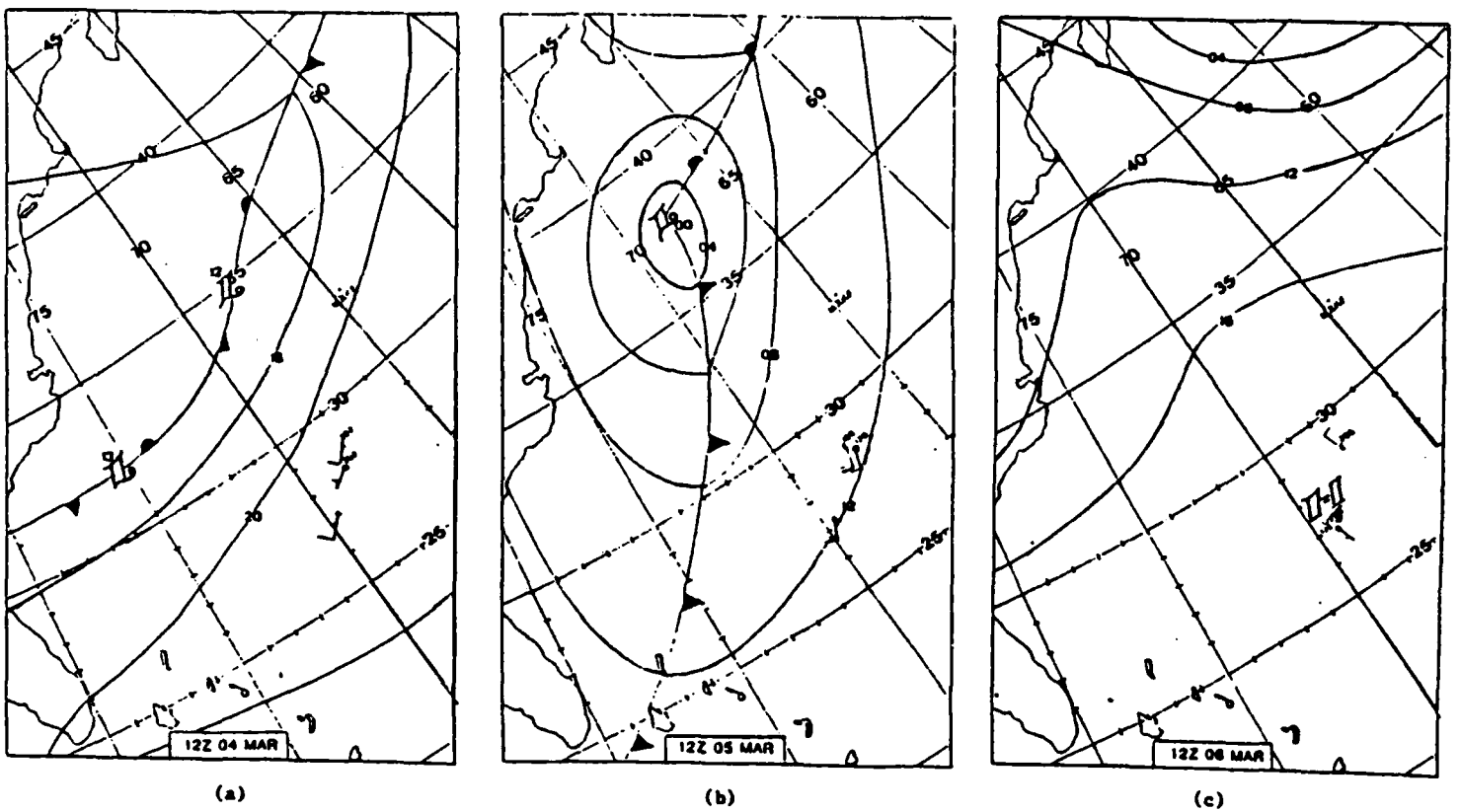

Fig. 4.22 Sea-level Pressure Maps for 4 Mar (a), 5 Mar (b), 6 Mar (c) 1986.

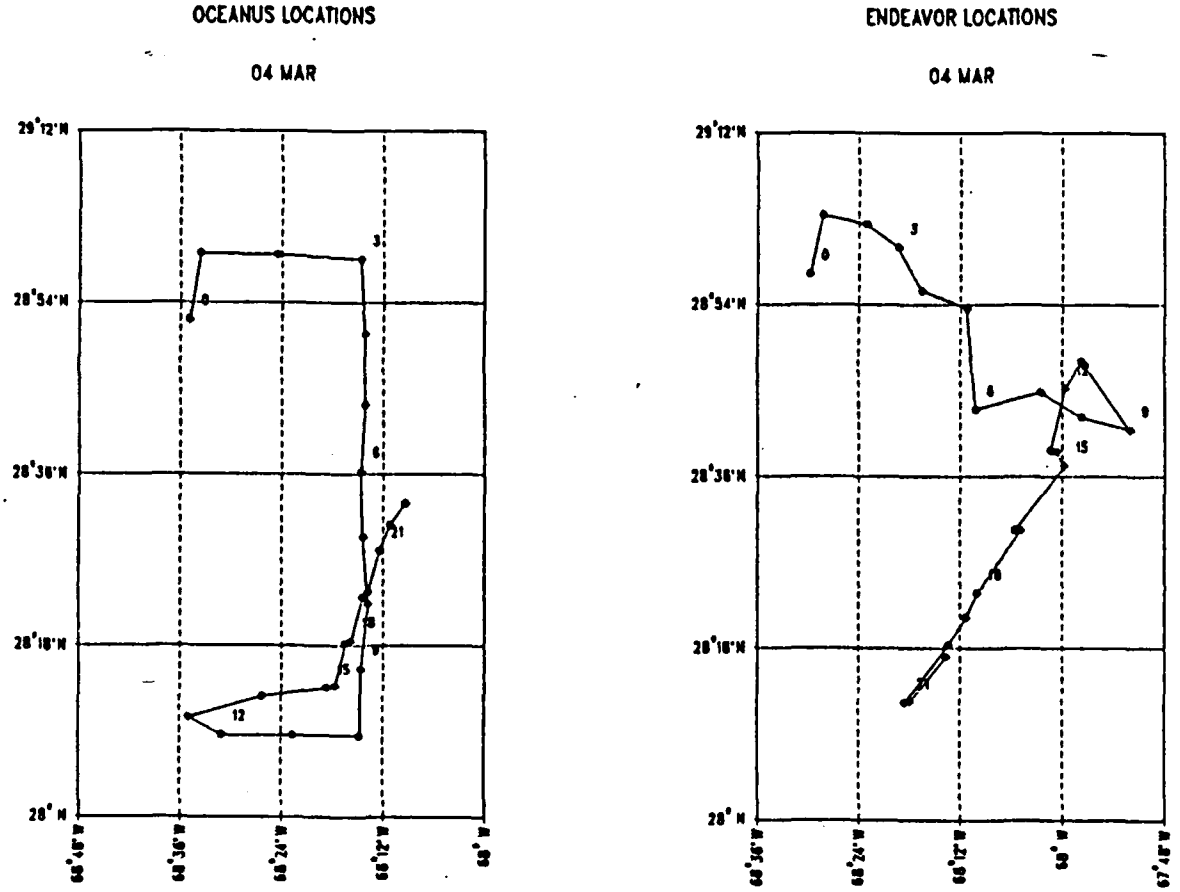

(a) (b)

Figure 4.23 Oceanus (a) and Endeavor (b) tracks for 4 March.

and its associated cold front passed the Oceanus at 2030 UT, the Endeavor at 2115 UT on 5 March. The Oceanus experienced a 1.7° C decrease in air temperature, and the Endeavor a 1.2° C decrease. Both ships recorded a wind shift from southwest to northwest as the front passed. Wind speeds reached a maximum of 14 ms^{-1} at the frontal passage, and sea-level pressure decreased to a minimum of 1013 mb. For the remainder of 5 March, winds remained northwesterly and gradually decreased to 10-11 ms^{-1}. Cloud cover consisted of altostratus and cirrus, giving way to partial clearing before the frontal passage and low level stratus afterward. Light rain occurred at 0100 UT and 0800 UT.

The swell 0000 UT on 5 March was from the southwest with an observed height of 7 ft. It increased and shifted to the south by 1200 UT. By the time of the frontal passage, swell heights had increased to 12 ft, and the direction had shifted back to the southwest.

The Oceanus and the Endeavor followed somewhat erratic tracks during 5 March (Fig. 4.24). The Oceanus, however, remained near one station for several hours surrounding the frontal passage.

Weak high pressure built behind the front on 6 March, resulting in a sea-level pressure increase from 1017 mb to 1021 mb during the day. Wind direction remained from the northwest and wind speed decreased to 1-3 ms^{-1} by 1200 UT. Swell direction shifted to the northwest by 0400 UT and swell height decreased to 2-3 ft by 2400 UT. Cloud cover was patchy stratus and altostratus.

The ship tracks for 6 March are shown in Fig. 4.25. The Oceanus moved steadily southwest away from the front. The Endeavor followed a more complicated path centered near one station.

2. **Frontal Cross-sections for the Frontal Passage of 5 March**

The cross-sections for the 5 March frontal passage are shown in Fig. 4.26. The Oceanus stress ratio cross-section is the one presented because the Endeavor cross-section, though similar in trend, contains several apparent outliers and is considered less representative.

The pattern shown in these cross-sections is similar to that in several of the other frontal passages. Low values of the stress ratio well ahead of the front correspond with low wind speeds (generally less than 6 ms^{-1}) and low wind-swell direction differences. A packet of northwesterly propagating swell passed though the region between 1700 UT and 2000 UT on 4 March, increasing the wind-swell direction

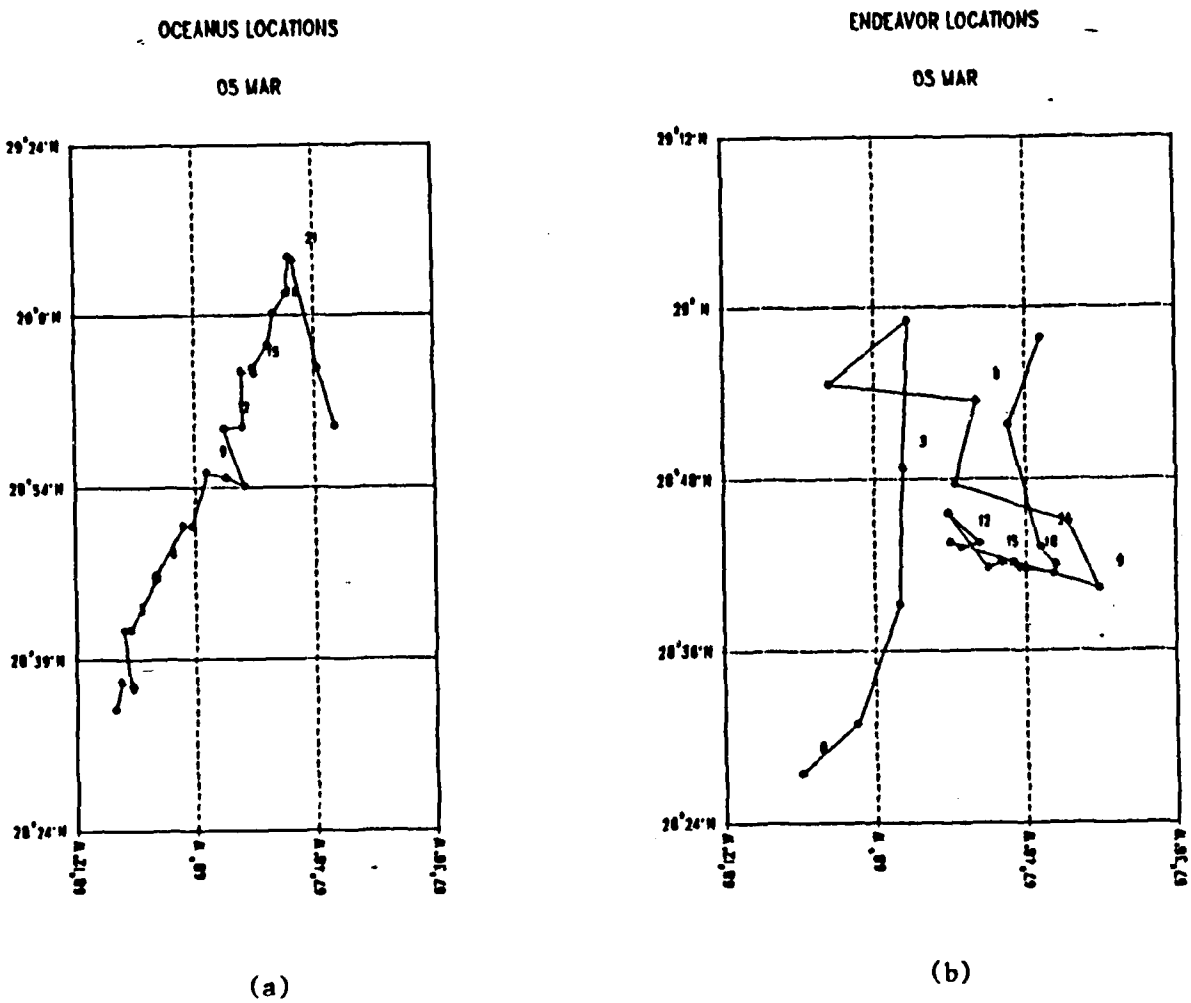

(a) (b)

Fig. 4.24 Oceanus (a) and Endeavor (b) tracks for 5 March 1986.

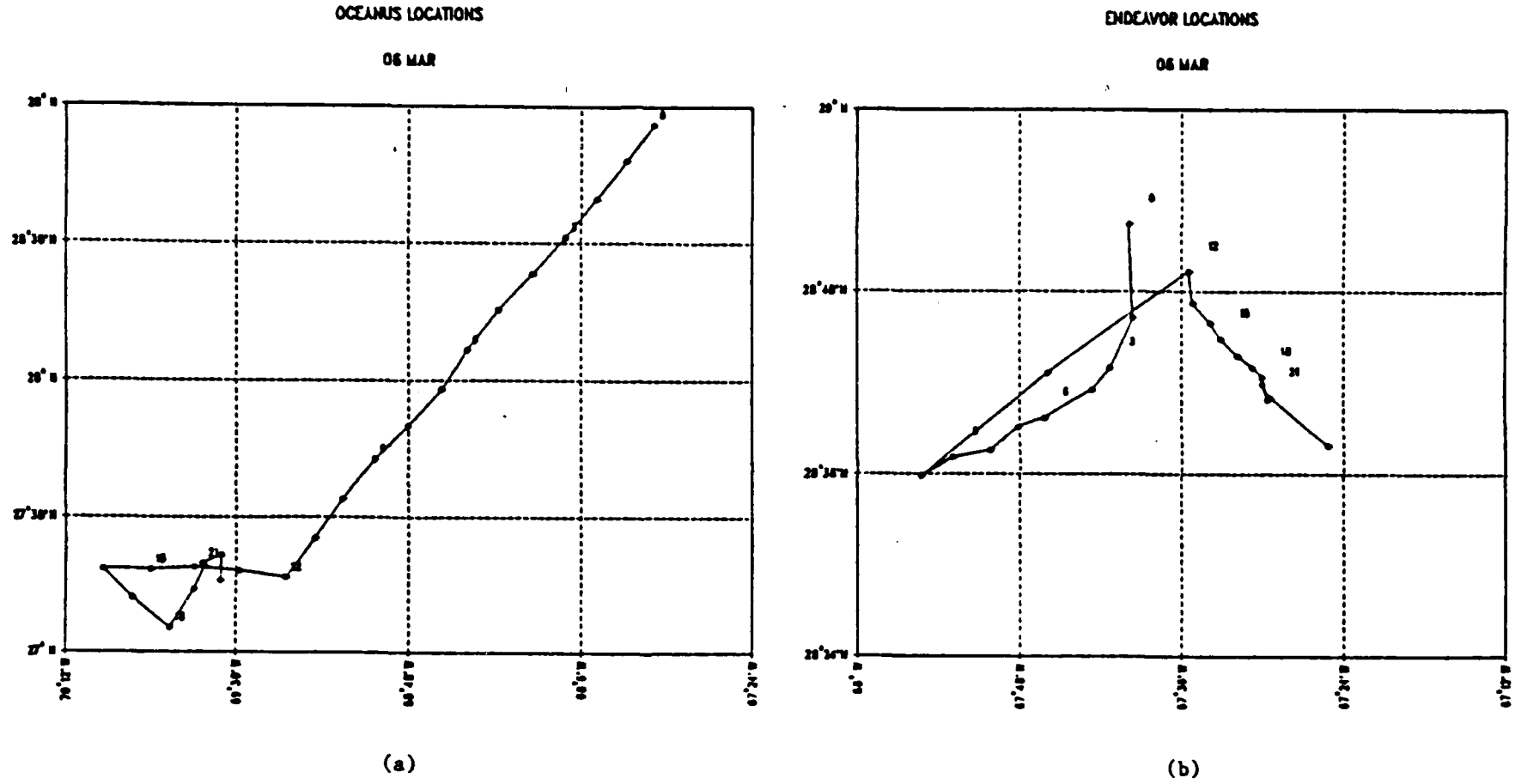

Fig. 4.25 Oceanus (a) and Endeavor (b) tracks for 6 March 1986.

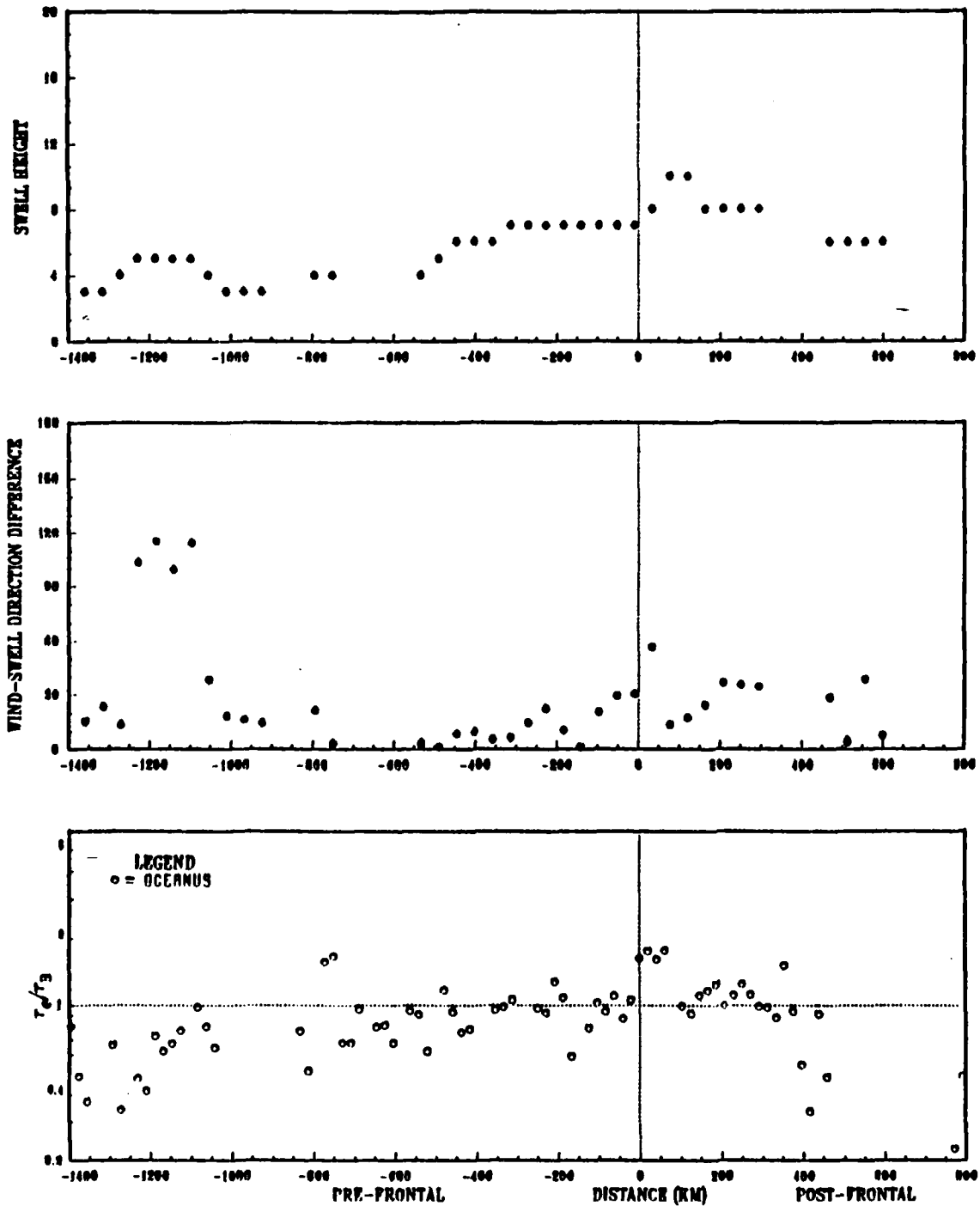

Fig. 4.26 Frontal cross-sections for the frontal passage of 5 March 1986.

difference from 15 degrees to nearly 120 degrees, but swell heights were low (5 ft), and there seems to have been little effect on the stress ratios.

A minor increase in the stress ratio, with a peak value of 1.3, occurred 200 km ahead of the front. This coincides with an increase in swell height (from 6 to 7 ft) and an increase in wind-swell direction difference as the swell direction shifted from south to southwest. Winds were fairly constant at 8-10 ms^{-1}. This episode appears related to radiation of swell from behind the front.

A more pronounced enhancement occurred just after the frontal passage, with a peak stress ratio of 1.6 to 1.8 in the region from the frontal passage to 60 km behind the front. This occurred as the wind direction shifted from southwest to northwest and wind speed increased to 12-14 ms^{-1} during the frontal passage, while the swell direction shifted more slowly to the west. The wind-swell direction difference again correlates well with the stress enhancement. This appears to be a case of wind-wave modulation by the underlying swell. The swell heights again increase only after the stress enhancement becomes evident. In this case, the swell height peak occurred approximately 2.5 h after the stress ratio peak.

V. COMPOSITE RESULTS

The stress ratios from the Oceanus and the Endeavor, respectively, composited over the six frontal passages, appear in Figs. 5.1 and 5.2. The upper graph in each figure includes all points for each ship; the lower graph shows the means in 100-km range bins. The vertical bars in the lower graph represent the uncertainty in the means; the numbers above the plotted points show the number of data points in each range bin.

Considerable scatter is evident in both ships' plots. However, the clear pattern seen in the means is also discernible in the multi-point plots. While the magnitudes differ slightly, the same stress ratio trends occur at the same distances in each ship's data.

A general feature for both ships is that the mean stress ratios are centered near or slightly below 1.0 in the region extending from 1400 km to about 400 km ahead of the front, except for a minor enhancement peak which occurs in the region near 850-800 km ahead of the front. This peak was related to wave convergence ahead of a surface trough for the 20 February frontal passage. The peak is also evident in several of the other frontal passage cases, though the mechanisms responsible were not as clear in these cases.

Both plots show a strong enhancement peak centered near the frontal passage and extending at least 400 km on either side of the front. The mean stress ratios for the Endeavor reach a peak value of 1.4, those for the Oceanus a peak of nearly 1.6. This enhancement appears to be induced by wave convergence ahead of the front. The energetic sea state created by this mechanism apparently persists for some time after the front passes and the wind and waves become nearly parallel. This may be evidence of the dynamic wave modulation mechanism. As the post-frontal distance increases further, the stress ratios return to near 1.0. The Oceanus values in this area decrease to well below 1.0, but the means are based on very few data points. The Endeavor values appear more representative at this range.

Fig. 5.3 shows the composite for the six storms of the stress ratios from both ships. The trends discussed above are clearly evident in the means, although the scatter of points is relatively large.

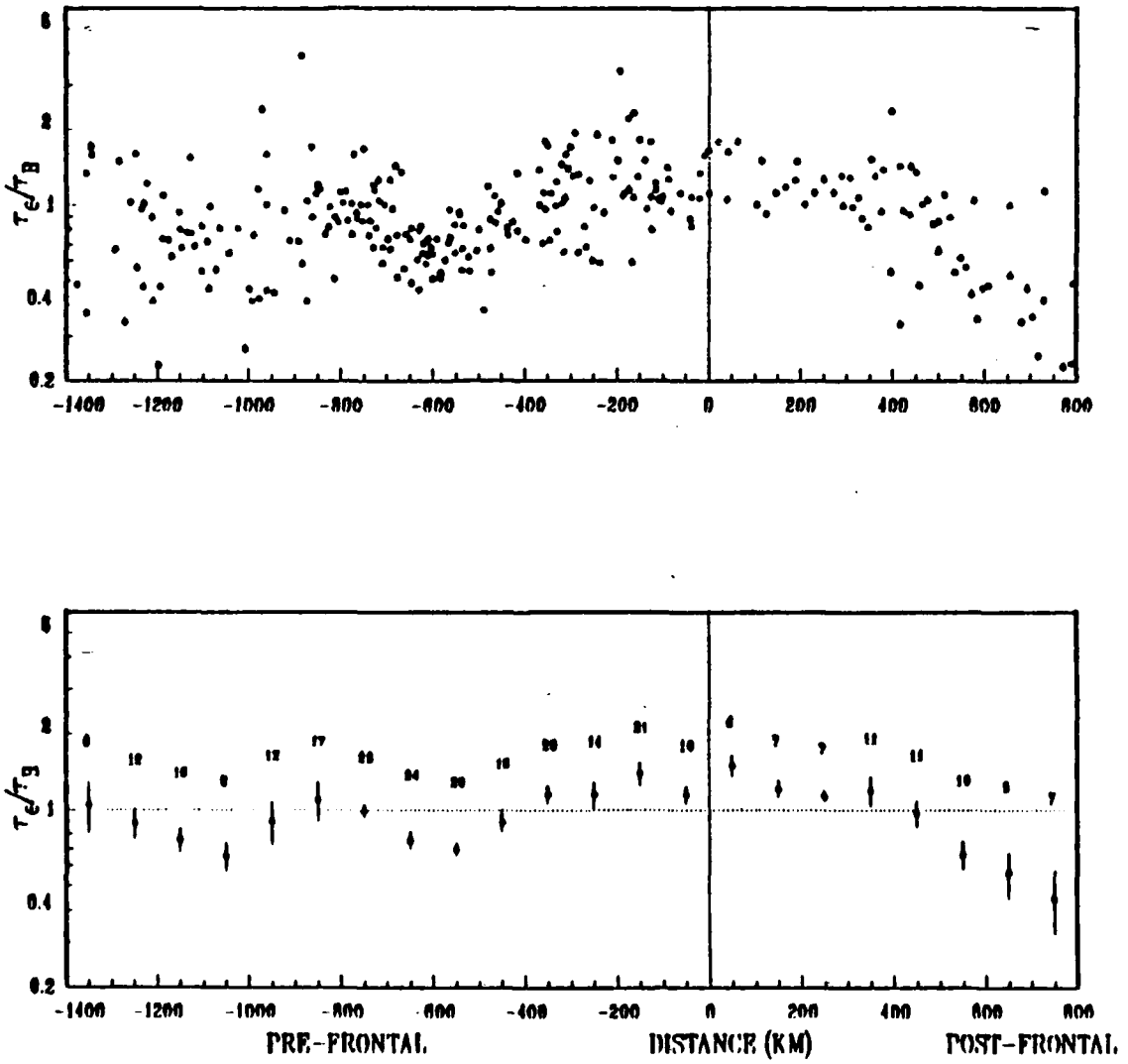

Fig. 5.1 Six-storm composite of Oceanus stress ratios.

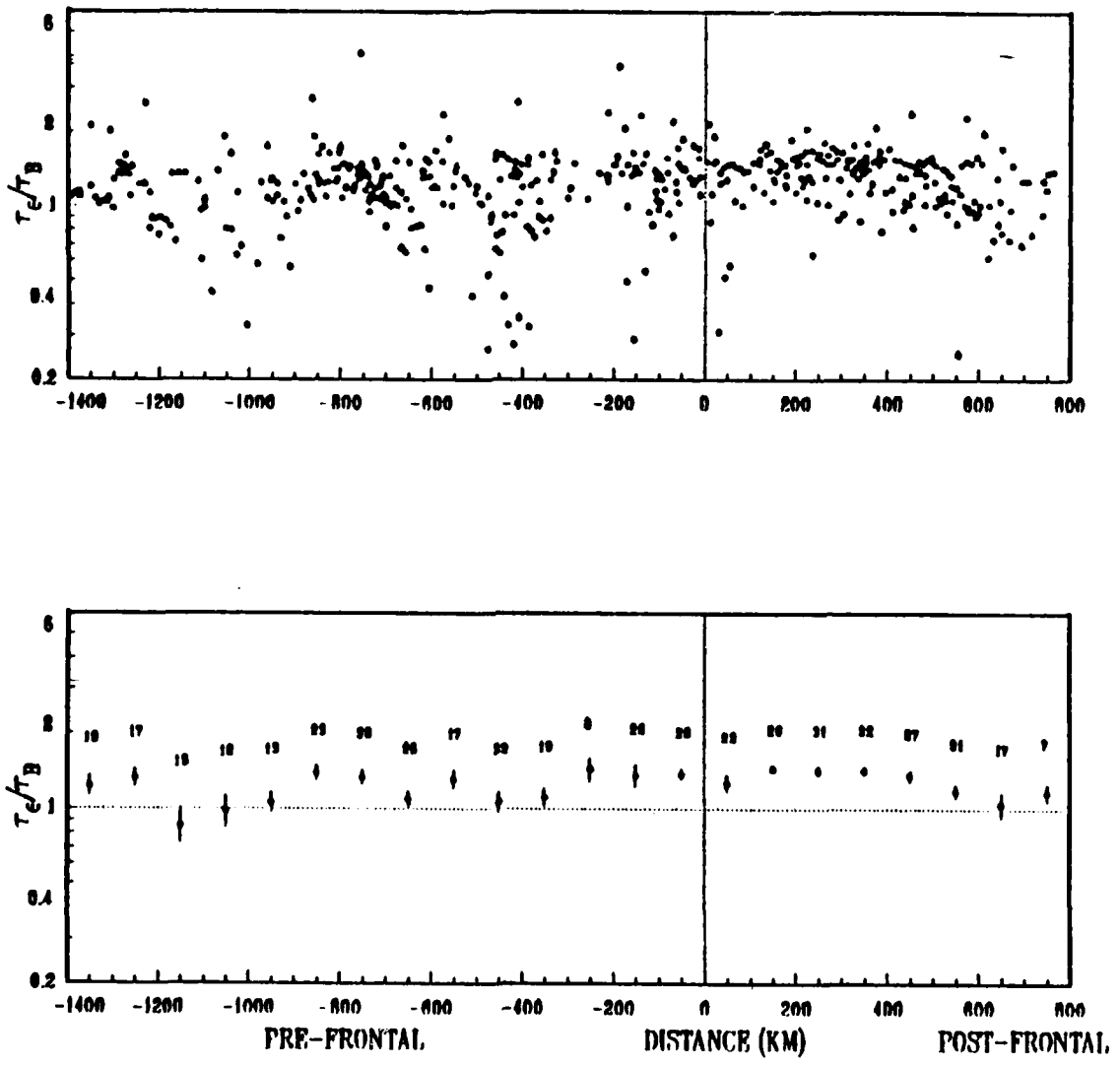

Fig. 5.2 Six-storm composite of Endeavor stress ratios.

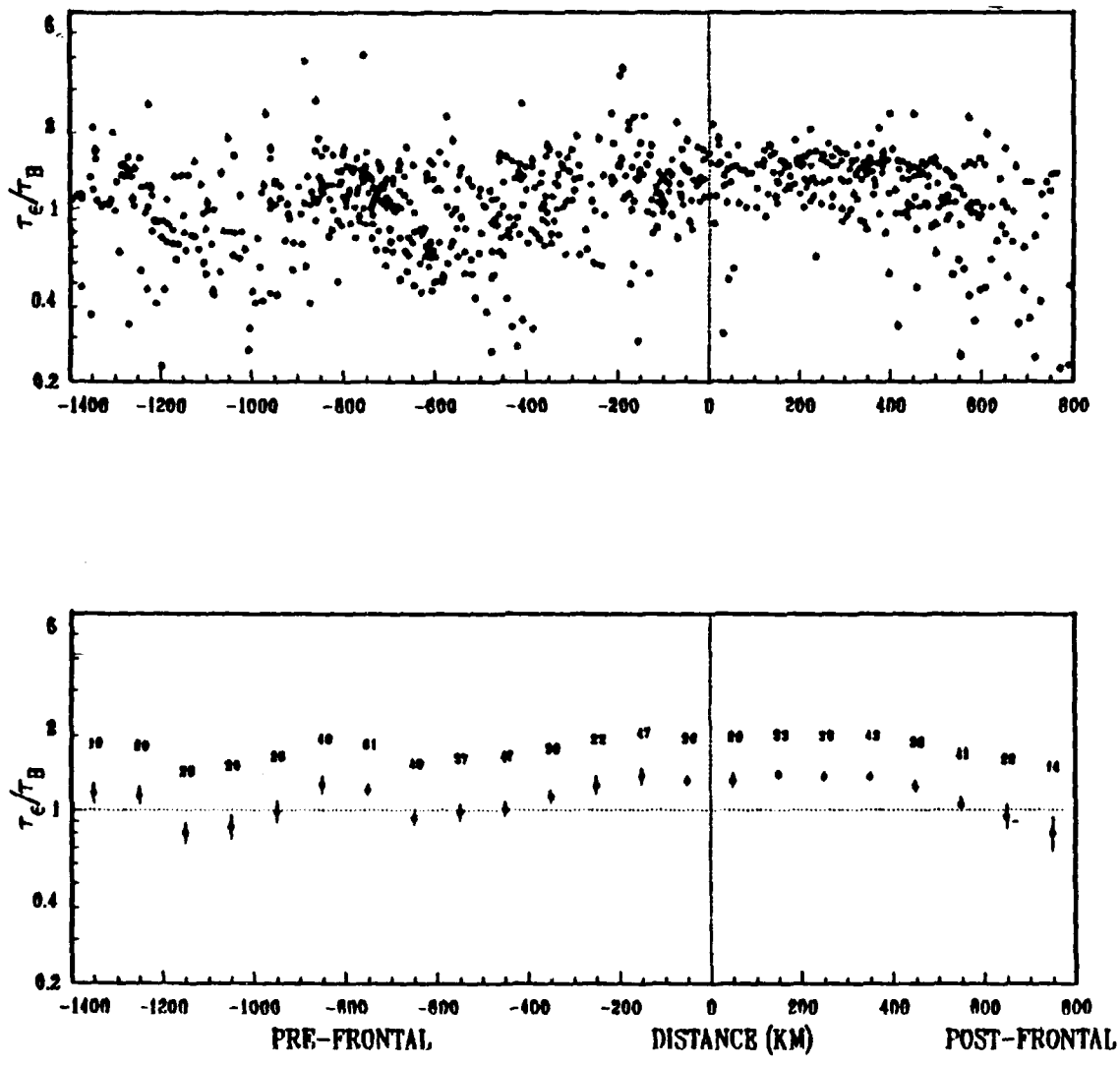

Fig. 5.3 Six-storm composite of stress ratios from both ships.

Neutral drag coefficients, C_{dn}, for the 10 meter level were calculated from the ship dissipation derived friction velocity, u_*, and wind speed, u_{10}, values. The C_{dn} results presented are from data which had been edited on the basis of criteria described in Chapter III. It is believed that results selected with these criteria and properly corrected for stability effects are suitable for evaluating the dependence of C_{dn} on wind speed.

C_{dn} versus u_{10} results for the two sensor types (hot film and propellor) on the two ships are shown in Fig. 5.4. The plotted values represent arithmetic means within .5 ms^{-1} intervals. The C_{dn} versus wind speed formulation of Large and Pond (1981) is shown for comparison as a solid line, with ± 30 per cent variations indicated by dotted lines. The lower graph shows the results for the individual sensors, the upper graph composite means from all sensors.

Over the u_{10} range from 4 to 11 m^{-1}, the mean values, representing large samples for each set, agree well ($\pm 30\%$) with the Large and Pond value of 1.2×10^{-3}. Differences of more than $\pm 10\%$ are most evident in the 4 to 6 ms^{-1} range for the Oceanus hot film and 8.5 to 9.5 ms^{-1} range for the Endeavor hot film. The composite set C_{dn} value for $4 < u_{10} < 11$ ms^{-1} is 1.21×10^{-3}.

For $u_{10} > 11$ ms^{-1}, the Oceanus results are inconclusive and the Endeavor hot film results increase more quickly with wind speed than the Large and Pond formulation. This could be due to non-removed wind-wave coupling effects which are most pronounced with high wind speeds associated with atmospheric frontal passages.

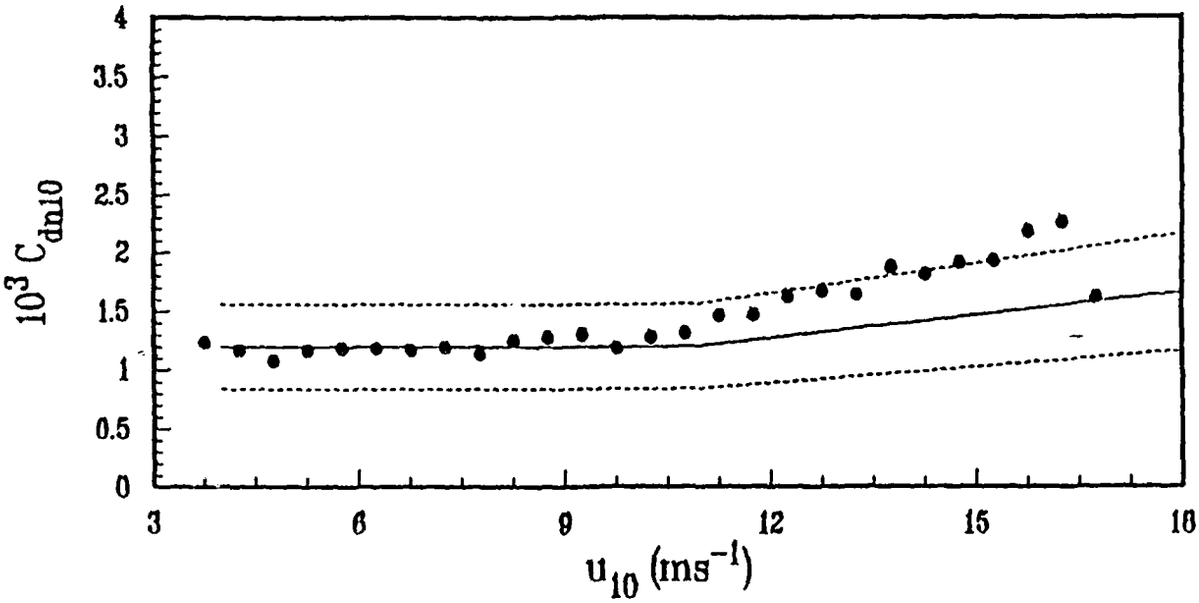

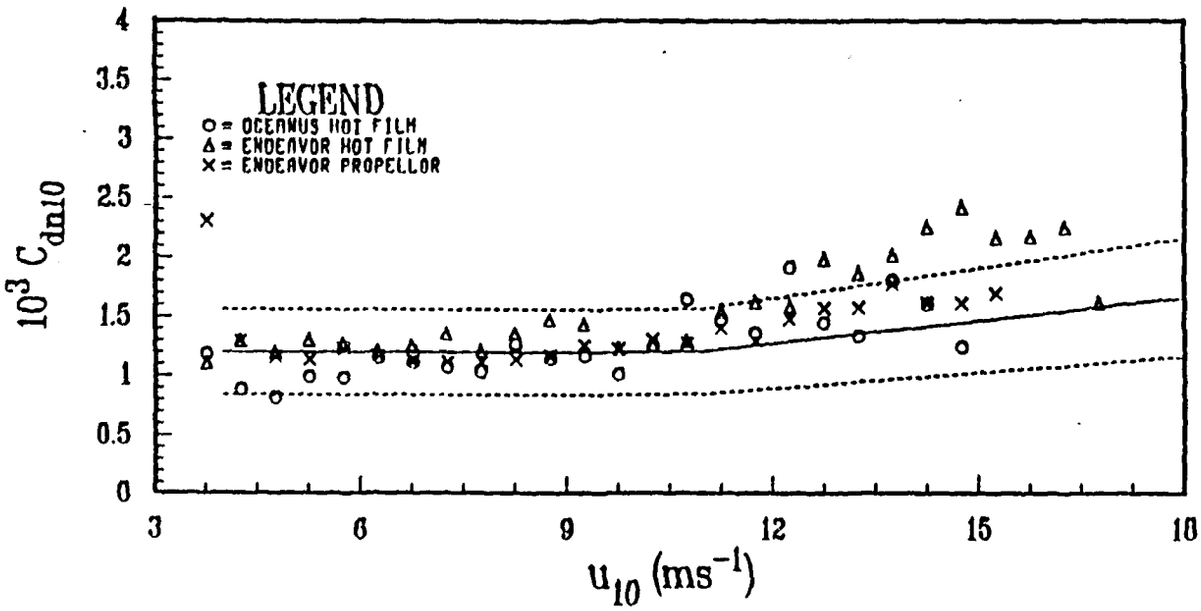

Fig. 5.4 10-m Neutral Drag Coefficients as a Function of 10-m Wind Speed Individual Sensors (a) and Composite (b).

VI. CONCLUSIONS

The stress ratio results clearly demonstrate the inadequacy of existing stability- and wind speed-dependent drag coefficient parameterizations for determining the wind stress variations occurring near an atmospheric front. Dissipation stresses significantly higher than those obtained by the bulk method were associated with all six frontal passages during FASINEX 1986. Ratios of dissipation to bulk stress as high as 3.6 were observed in this data set. In the mean over six storms, stress enhancement was evident within 400 km on either side of the front, with mean stress ratios of 1.3 to 1.5 within 200 km of the front. Although it is not evident in the composite results, dissipation stresses significantly lower than the bulk stress were also observed in several cases.

Changes in the stress ratio tended to coincide with swell height changes when the wind-swell direction differences were small or constant. This is apparently evidence of the effect of dynamic wave modulation on the wind stress.

The largest stress ratio enhancements were ascribed to wave convergence ahead of the front caused by radiation of swell through the front from the cold sector. Substantial reductions in the stress ratio were seen on two occasions to coincide with a train of swell whose direction was nearly opposite the wind direction propagating through the region.

Some of the stress ratio variations observed in this data set cannot be clearly explained in terms of either of the mechanisms proposed by Geernaert, *et al.* (1986b). Evidence of these mechanisms is seen in the data, but some of the stress variations do not appear from the data available to be related to either mechanism discussed.

The variations of wind stress with distance from the front seen in this study are quite similar to those observed by Boyle, *et al.* (1987) in the North Atlantic during MIZEX, and by Geernaert, *et al.* (1986b) in the North Sea during MARSEN. Each of those studies was based on observations of one or two frontal passages, with limited or no wave data. This study, covering six frontal passages and using a more extensive set of wave data, shows many of the same features observed by the previous investigators. Furthermore, the wave data gives some indication that the mechanisms proposed by Geernaert, *et al.* (1986b) do affect the wind stress near a front.

This investigation, however, leaves many unanswered questions and much room for further study. The use of single hourly wave observations made by an observer on the bridge, for example, is an obvious limitation. Future studies should couple observations of the complete directional wave spectrum with stress observations. This would permit evaluation of the current sea state dependent drag coefficient formulations in near-frontal situations and add to our understanding of the processes leading to stress enhancement near a front. It also appears that more theoretical and laboratory work is needed to identify and quantify the mechanisms leading to the stress enhancement.

LIST OF REFERENCES

Boyle, P. J., K. L. Davidson, and D. E. Spiel, 1987. Characteristics of overwater stress during STREX. *Dyn. Atm. Oceans, 10(4)*: 343-358.

Businger, J. A., J. C. Wyngaard, and Y. Izumi, 1971. Flux profile relationships in the atmospheric surface layer. *J. Atmos. Sci., 28*: 181-189.

Byrne, H. M., 1982. *The Variations of the Drag Coefficient in the Marine Surface Layer due to Temporal and Spatial Variations in the Wind and Sea State.* Ph.D. Dissertation, University of Washington, 119 pp.

Champagne, F. H., C. A. Friehe, D. C. la Rue, and J. C. Wyngaard, 1977. Flux measurements, flux estimation techniques, and fine-scale turbulence measurements in the atmospheric surface boundary layer. *J. Atmos. Sci., 34*: 513-530.

Charnock, H., 1955. Wind stress on a water surface. *Quart. J. Roy. Meteor. Soc., 81*: 639-640.

Donelan, M. A., 1982. The dependence of the aerodynamic drag coefficient on wave parameters. In: *First International Conference on Meteorology and Air-Sea Interaction of the Coastal Zone.* Am. Meteorol. Soc., Boston, pp. 381-387.

Geernaert, G. L., 1987. On the importance of the drag coefficient in air-sea interactions. *Dyn. Atmos. Oceans, 11*: 19-38.

Geernaert, G. L., K. L. Davidson, and P. J. Boyle, 1986a. Variation of the drag coefficient and wind-wave coupling in the vicinity of a storm front. Unpublished manuscript.

Geernaert, G. L., K. B. Katsaros, and K. Richter, 1986b. Variation of the drag coefficient and its dependence on sea state. *J. Geophys. Res., 91(C6)* : 7667-7679.

Guest, P. S., and K. L. Davidson, 1987. The effect of observed ice conditions on the drag coefficient in the summer East Greenland Sea marginal ice zone. *J. Geophys. Res., 92(C7)*: 6943-6954.

Haltiner, G. J., and R. T. Williams, 1980. *Numerical Prediction and Dynamic Meteorology.* John Wiley and Sons, Inc., New York, 477 pp.

Hsu, S. A., 1974. A dynamic roughness equation and its application to wind stress determination at the air-sea interface. *J. Phys. Oceanogr., 4*: 116-120.

Kitaigorodskii, S. A., 1973. *The Physics of Air-Sea Interaction*, translated from the Russian by A. Baruch, Israel Program for Scientific Translations, Jerusalem, 237 pp.

Large, W. G., and S. Pond, 1981. Open ocean momentum flux measurements in moderate to strong winds. *J. Phys. Oceanogr., 11*: 324-336.

McBean, G. A., and J. A. Elliot, 1975. The vertical transport of kinetic energy by turbulence and pressure in the boundary layer. *J. Atmos. Sci., 32*: 753-766.

Pennington, N. J., and R. A. Weller, 1986. Cruise summaries for FASINEX Phase Two, FASINEX Technical Report #14. *WHOI Technical Report 86-36*, Woods Hole Oceanographic Institution, Woods Hole, MA, 173 pp.

Phillips, O. M., and M. L. Banner, 1974. Wave breaking in the presence of wind drift and swell. *J. Fluid Mech., 66(4)*: 625-640.

Skupniewicz, C. E., S. H. Borrmann, S. R. Fellbaum, W. J. Shaw, C. A. Vaucher, and G. T. Vaucher, 1986. Shipboard Observations of Mean and Turbulent Atmospheric Surface Layer Quantities, SCCAMP Data Report, Part 1. *NPS Technical Report.*

Wyngaard, J. C., and O. R. Cote, 1971. The budgets of turbulent kinetic energy and temperature variance in the atmospheric surface layer. *J. Atmos. Sci., 28*: 190-201.

INITIAL DISTRIBUTION LIST

		No. Copies
1.	Defense Technical Information Center Cameron Station Alexandria, VA 22304-6145	2
2.	Library, Code 0142 Naval Postgraduate School Monterey, CA 93943-5002	2
3.	Chairman, Code 68Co Department of Oceanography Naval Postgraduate School Monterey, CA 93943-5000	1
4.	Chairman, Code 63Rd Department of Meteorology Naval Postgraduate School Monterey, CA 93943-5000	1
5.	Professor K. L. Davidson, Code 63Ds Department of Meteorology Naval Postgraduate School Monterey, CA 93943-5000	5
6.	Professor W. J. Shaw, Code 63Sr Department of Meteorology Naval Postgraduate School Monterey, CA 93943-5000	1
7.	LCDR James F. Mundy 4717 S. Rockford Drive Tempe, AZ 85282	3
8.	Director Naval Oceanography Division Naval Observatory 34th and Massachusetts Avenue NW Washington, DC 20390	1
9.	Commander Naval Oceanography Command NSTL Station Bay St. Louis, MS 39522	1
10.	Commanding Officer Naval Oceanographic Office NSTL Station Bay St. Louis, MS 39522	1

11.	Commanding Officer Fleet Numerical Oceanography Center Monterey, CA 93943	1
12.	Commanding Officer Naval Ocean Research and Development Activity NSTL Station Bay St. Louis, MS 39522	1
13.	Commanding Officer Naval Environmental Prediction Research Facility Monterey, CA 93943	1
14.	Chairman, Oceanography Department U. S. Naval Academy Annapolis, MD 21402	1
15.	Chief of Naval Research 800 N. Quincy Street Arlington, VA 22217	1
16.	Office of Naval Research, Code 420 Naval Ocean Research and Development Activity 800 N. Quincy Street Arlington, VA 22217	1
17.	Commander Oceanographic Systems Pacific Box 1390 Pearl Harbor, HI 20360	1
18.	Commander, Air-370 Naval Air Systems Command Washington, DC 20360	1
19.	Chief, Ocean Services Division National Oceanic and Atmospheric Administration 8060 Thirteenth Street Silver Springs, MD 20910	1
20.	Commanding Officer Naval Eastern Oceanography Center Naval Air Station Norfolk, VA 23511	1
21.	Dr. Robert A. Weller Woods Hole Oceanographic Institution Woods Hole, MA 02543	1

22. Dr. Pat DeLeonibus
NOAA/NESDIS
Code E/RA 13
Suitland Professional Center
Washington, DC 20233 — 1

23. Dr. Carl Friehe
Mechanical Engineering
University of California, Irvine
Irvine, CA 92717 — 1

24. Dr. Gary Geernaert
Code 7913 S
Naval Research Laboratory
Washington, DC 20375 — 1

25. Dr. Bill Large
N.C.A.R.
P.O. Box 3000
Boulder, CO 80307 — 1

26. Dr. F. K. Li
Jet Propulsion Laboratory
MS 183-701
4800 Oak Grove Drive
Pasadena, CA 91109 — 1

27. Dr. Raymond Pollard
Institute of Oceanographic Sciences
Wormley, Godalming
Surrey GU8 5UB
England — 1

28. Dr. Steve Stage
Department of Meteorology
Florida State University
Tallahassee, FL 32301 — 1

29. Dr. William Cross
ONR Code 1122 PO
800 North Quincy St.
Arlington, VA 22217 — 1

30. Dr. Norden Huang
ONR Code 1122 PO
800 North Quincy St.
Arlington, VA 22217 — 1

END

FEB.

1988

DTIC